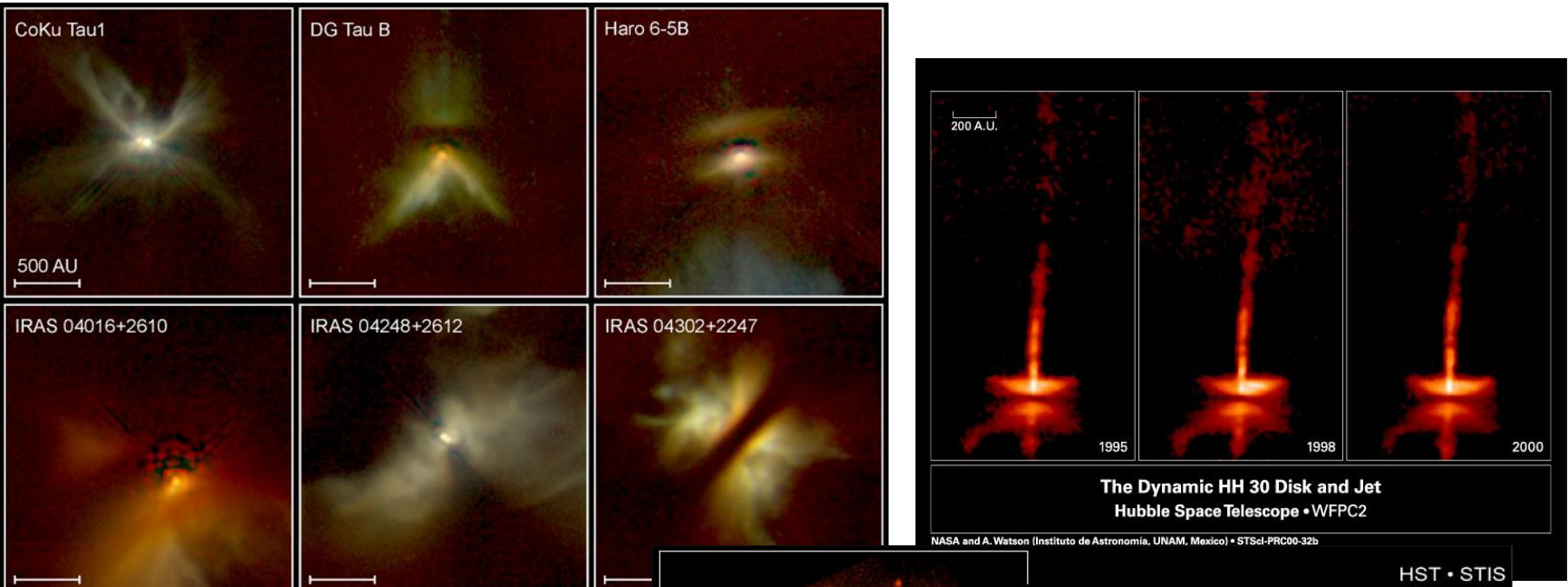


星・惑星系の形成過程 入門

中本泰史 (東工大)

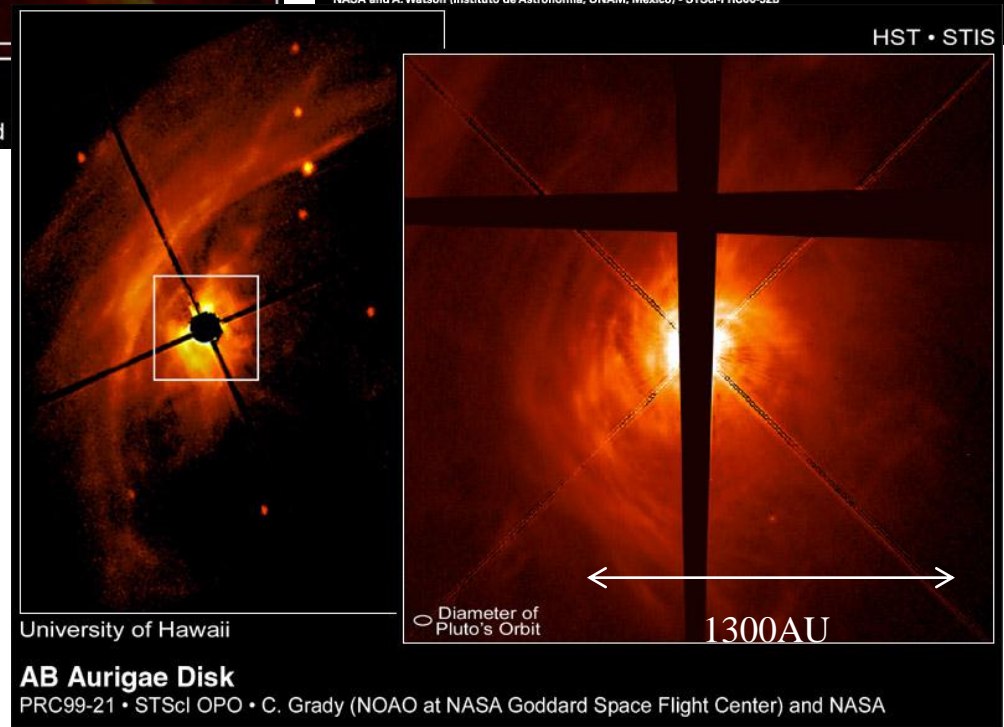
1. 形成過程の概観
2. 分子雲の重力収縮
3. 原始惑星系円盤
4. 固体微粒子の進化
5. 微惑星から惑星へ
6. 惑星系の形成



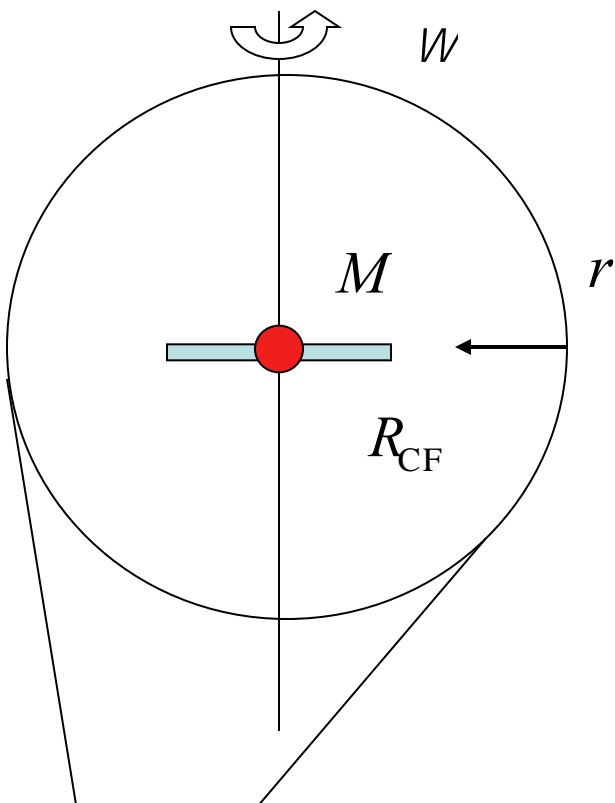
Young Stellar Disks in Infrared

PRC99-05a • STScI OPO
D. Padgett (IPAC/Caltech), W. Brandner (IPAC), K. Stapelfeldt (JPL) and

原始惑星系円盤



原始惑星系円盤の形成

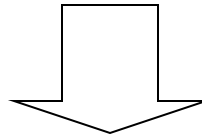


角運動量

$$j = r^2 W$$

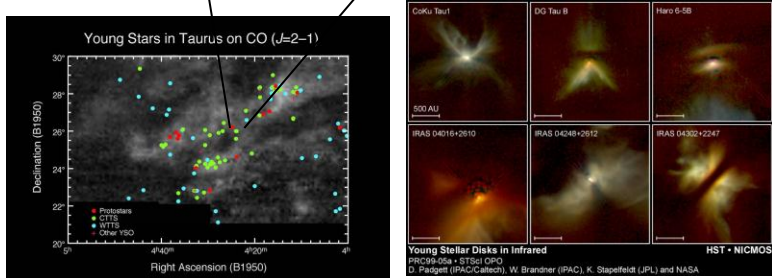
重力 = 遠心力

$$\frac{GM}{R_{\text{CF}}^2} = \frac{j^2}{R_{\text{CF}}^3}$$



$$R_{\text{CF}} = \frac{j^2}{GM} = \frac{r^4 W^2}{GM}$$

$$R_{\text{CF}} = 25 \times \frac{r}{10^4 \text{ AU}} \times \frac{W}{10^{-14} \text{ s}^{-1}} \times \frac{M}{M_{\text{sun}}} \text{ AU}$$



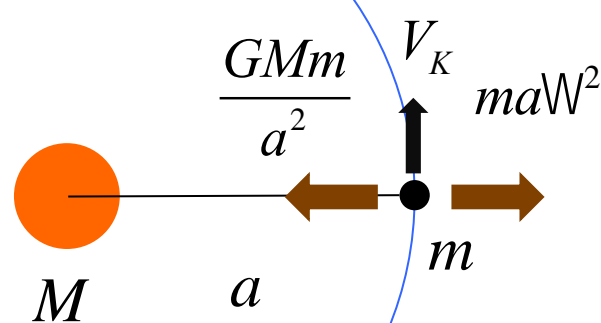
太陽(中心星)周りを回るもの力学の基礎

円盤ガス, 固体微粒子, 微惑星, 惑星, ...

円運動

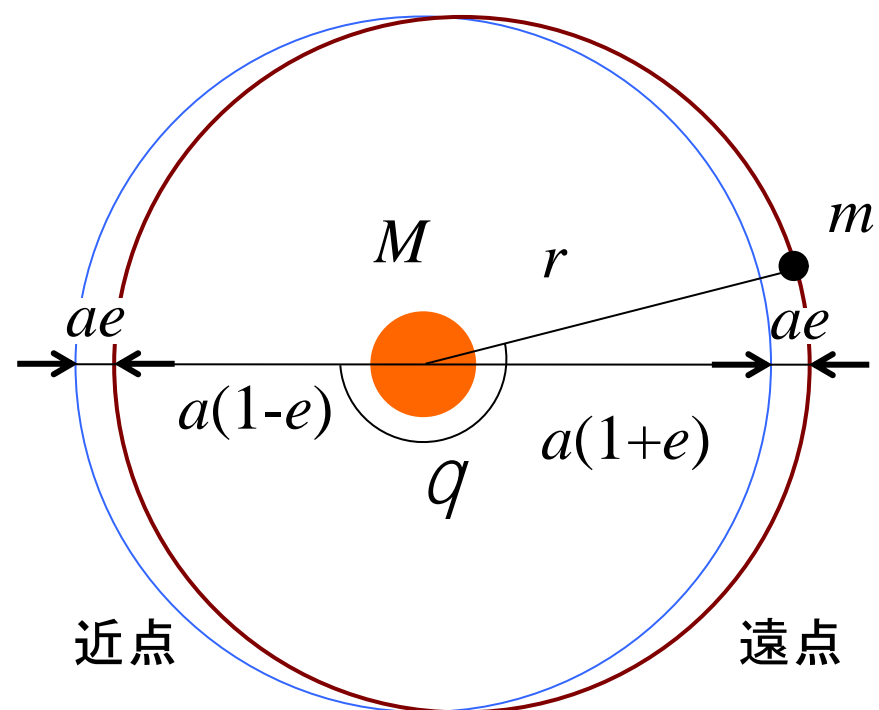
$$\frac{GMm}{a^2} = ma\mathbb{W}^2 \quad \Leftrightarrow \quad \mathbb{W}_K = \sqrt{\frac{GM}{a^3}} \quad \text{ケプラー回転角速度}$$

$$T_K = \frac{2\rho}{\mathbb{W}_K} = 2\rho \sqrt{\frac{a^3}{GM}} \quad \text{ケプラー周期}$$



$$V_K = a\mathbb{W}_K = \sqrt{\frac{GM}{a}} \quad \text{ケプラー速度}$$

橢円運動



a 軌道長半径
 e 離心率

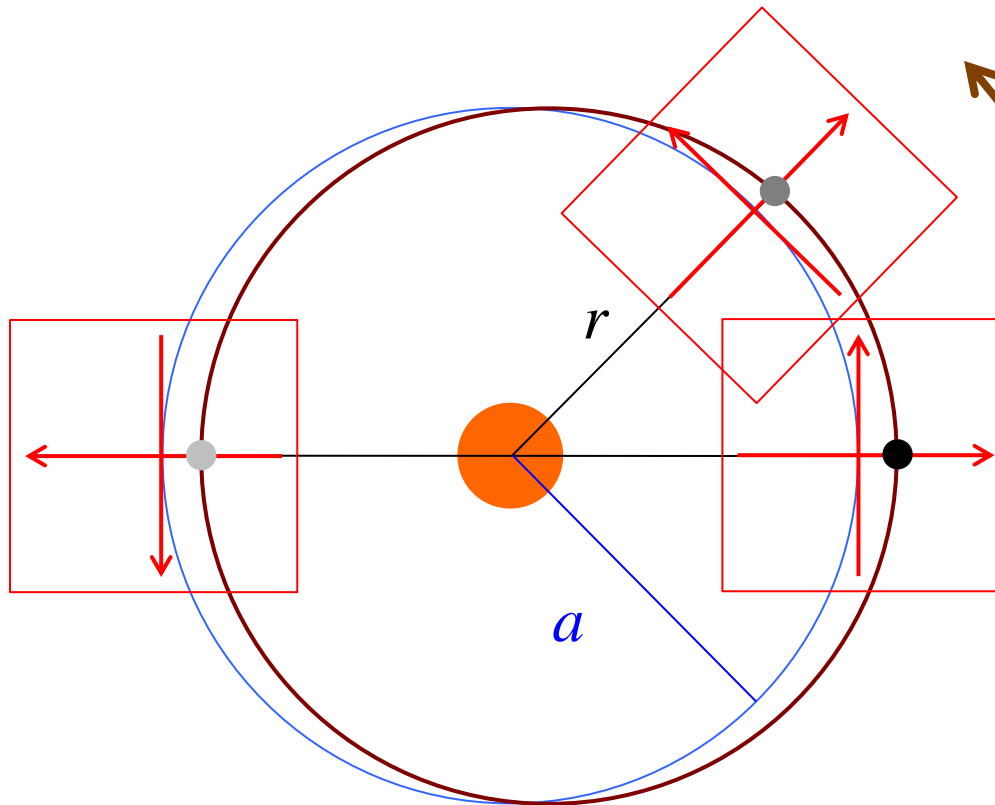
$$r = \frac{a(1 - e^2)}{1 + e \cos q}$$

$$E = -\frac{GMm}{2a}$$

力学的エネルギー

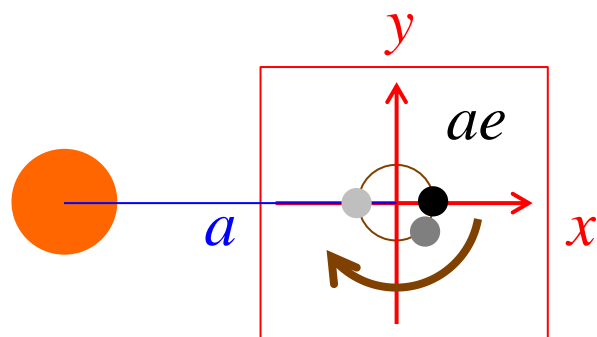
$$L = \sqrt{G \frac{M^2 m^2}{M + m} a (1 - e^2)}$$

角運動量



回転座標系

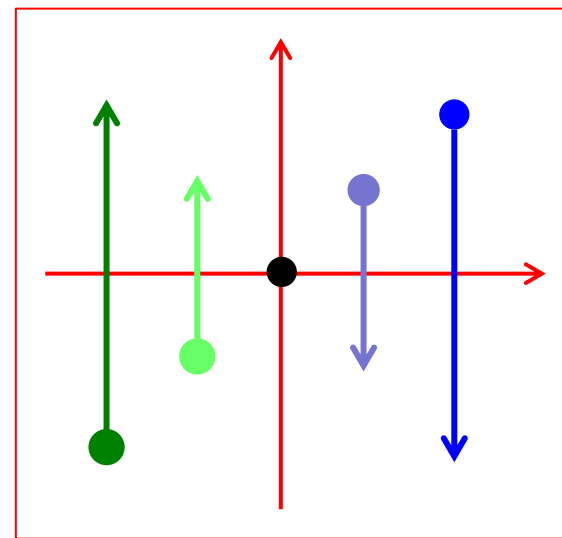
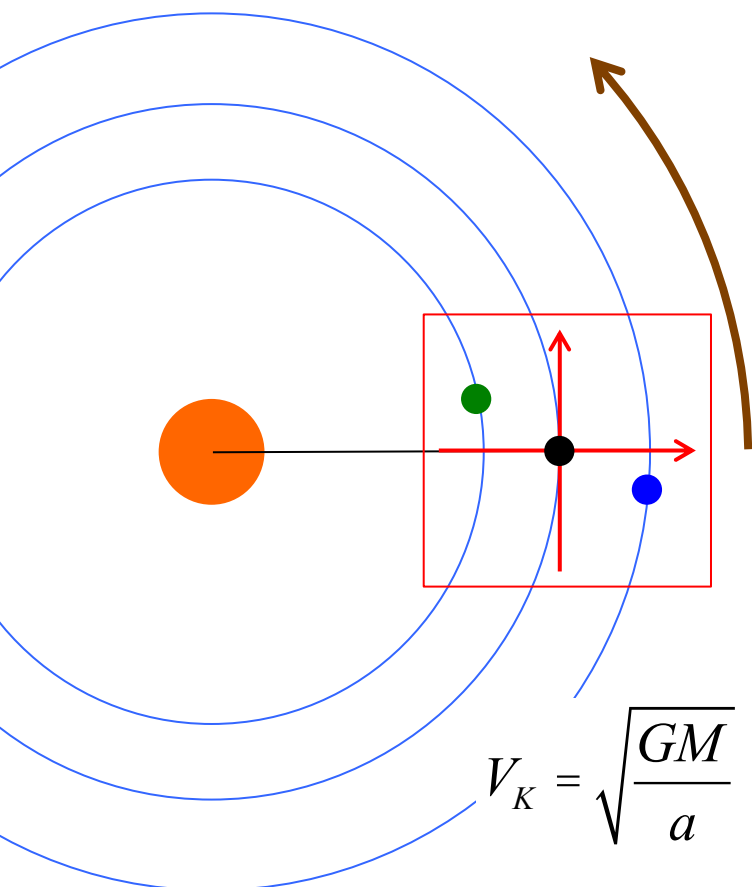
$$W_K = \sqrt{\frac{GM}{a^3}}$$



エピサイクル運動
(周転円運動)
周期 : T_K

$$v = aeW_K = V_K e$$

円運動の場合



$$\frac{dV_K}{da} = -\frac{1}{2} \sqrt{\frac{GM}{a^3}} = -\frac{1}{2} W_K$$

橙円運動の場合

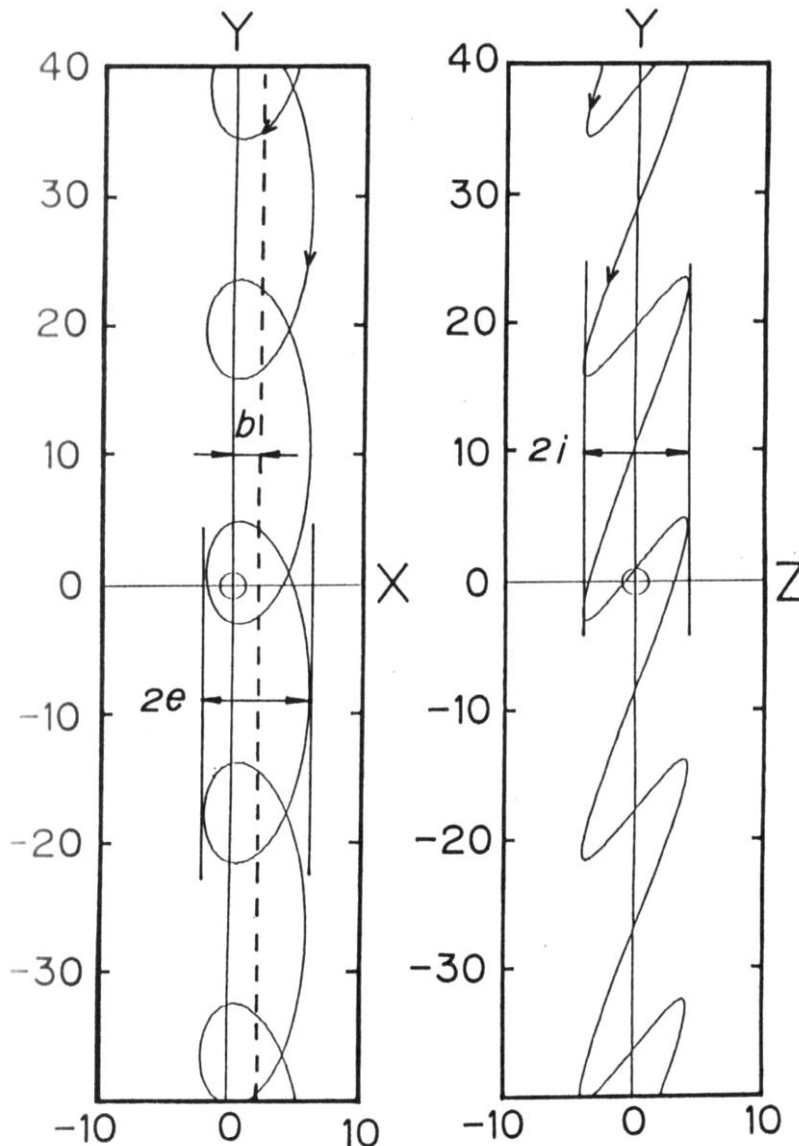
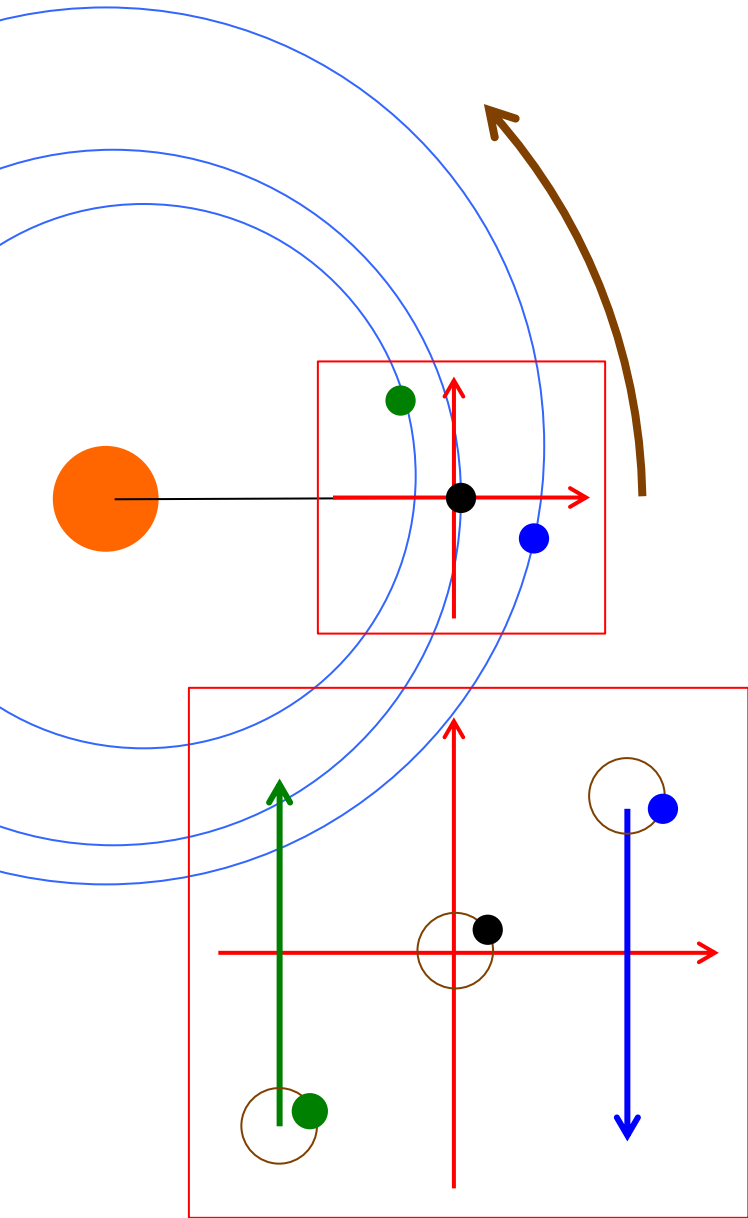


Fig. 2. A typical example of an unperturbed relative motion projected onto the x - y plane (left) and y - z plane (right). The circle at the origin denotes the Hill sphere. The dashed

重力相互作用する 2体の運動

Nishida 1983

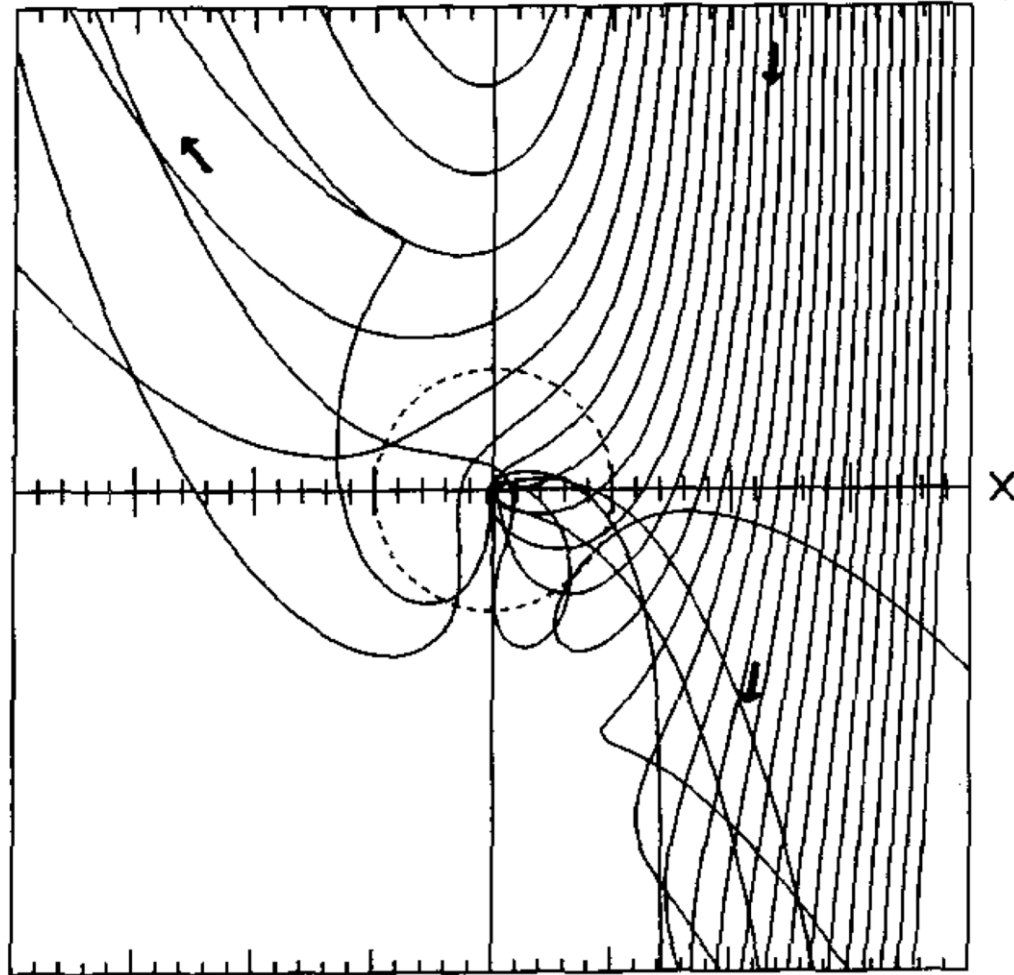
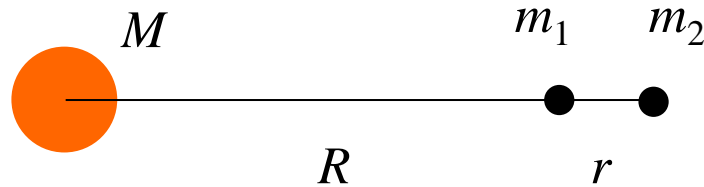


Fig. 2. Examples of particle orbits with various values of \tilde{b}_i and with $\tilde{e}_i=0$. The dotted circle represents the Hill sphere. All the particles with $1.75 < \tilde{b}_i < 2.50$ enter the sphere.

太陽による潮汐力



$$\frac{d^2r_1}{dt^2} = a_1 = -\frac{GM}{R^2}$$

$$\frac{d^2r_2}{dt^2} = a_2 = -\frac{GM}{(R+r)^2}$$

“1”を基準にしたとき, “2”に働く力

$$\Delta a_{21} = a_2 - a_1 = -\frac{GM}{(R+r)^2} + \frac{GM}{R^2} \approx +2\frac{GM}{R^3}r \quad \times m_2$$

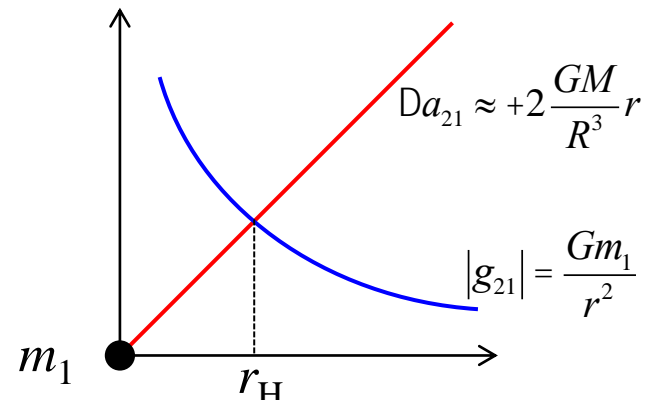
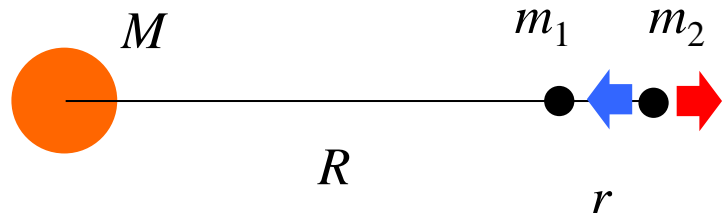
“2”を基準にしたとき, “1”に働く力

$$\Delta a_{12} = a_1 - a_2 = -\frac{GM}{R^2} + \frac{GM}{(R+r)^2} \approx -2\frac{GM}{R^3}r \quad \times m_1$$

(単位質量あたり)に働く“1”と“2”を引きはがす力

$$|\Delta a| \approx 2\frac{GM}{R^3}r = 2W_K^2r \quad \text{太陽による潮汐力}$$

質点“1”の重力圏



“1”を基準にして, “2”に働く潮汐力

$$Da_{21} \approx +2 \frac{GM}{R^3} r$$



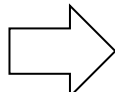
“1”が“2”に及ぼす重力

$$g_{21} = -\frac{Gm_1}{r^2}$$



潮汐力と重力が等しくなる距離は?

$$2 \frac{GM}{R^3} r = \frac{Gm_1}{r^2}$$

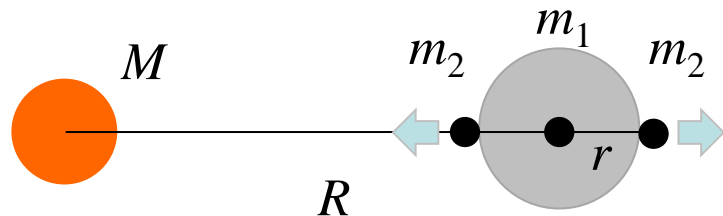


$$r_H = \sqrt[3]{\frac{m_1}{2M}} R$$

Hill半径

注：厳密な定義 $r_H = \sqrt[3]{\frac{m_1 + m_2}{3M}} R$

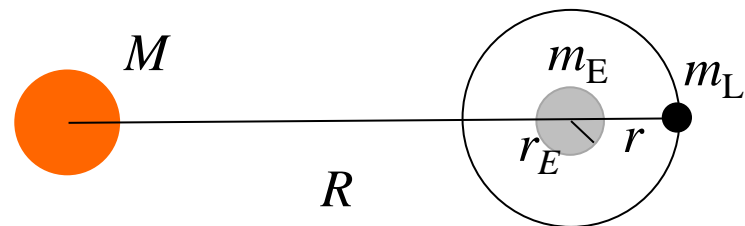
参考：地球に作用する潮汐力



$$|D\alpha| \approx 2 \frac{GM}{R^3} r = 2W_K^2 r$$

太陽-地球-月系の場合

地球に作用する潮汐力



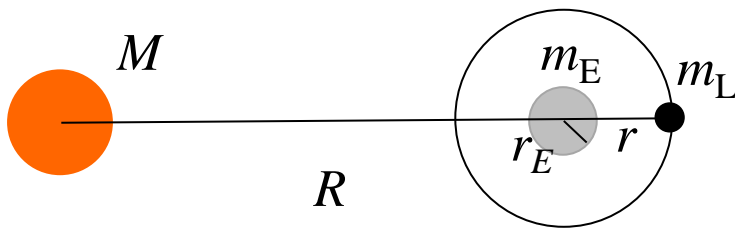
太陽から $|D\alpha_S| = 2 \frac{GM}{R^3} r_E$

月から $|D\alpha_L| = 2 \frac{Gm_L}{r^3} r_E$

$$\left| \frac{D\alpha_L}{D\alpha_S} \right| = 2 \frac{Gm_L}{r^3} r_E / 2 \frac{GM}{R^3} r_E = \left(\frac{R}{r} \right)^3 \frac{m_L}{M} \approx 2$$

月による潮汐力の方が大きい

月は地球の“重力圏”内にいるか？



月に作用する重力

$$\text{太陽} \quad g_S = -\frac{GM}{R^2}$$

$$\text{地球} \quad g_E = -\frac{Gm_E}{r^2}$$

$$\left| \frac{g_E}{g_S} \right| = \frac{m_E}{M} \frac{R^2}{r^3} \gg 0.4$$

太陽重力の方が強く月に作用している！

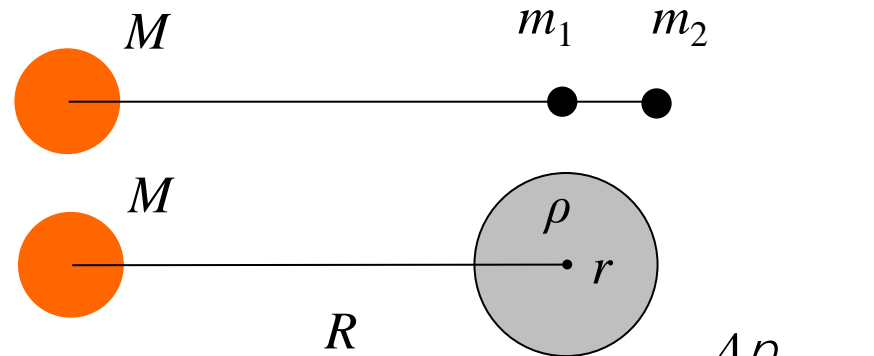
地球のHill半径

$$r_H = \sqrt[3]{\frac{m_E}{2M}} R = 1.7 \times 10^6 \text{ km}$$

$$r = 4 \times 10^5 \text{ km} \quad \text{地球-月距離}$$

月は地球のHill圏内にいる！

質量 m_1 の重力圏



m_1 を固定

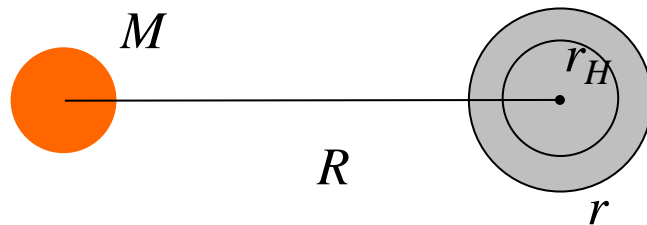
$$r = \frac{m_1}{\frac{4\rho}{3}r^3} \rightarrow \frac{m_1}{\frac{4\rho}{3}r_H^3} = \frac{m_1}{\frac{4\rho}{3}\frac{m_1}{2M}R^3} = \frac{2M}{\frac{4\rho}{3}R^3} \circ r_R$$

$$m_1 = \frac{4\rho}{3} r r^3$$

ρ を固定

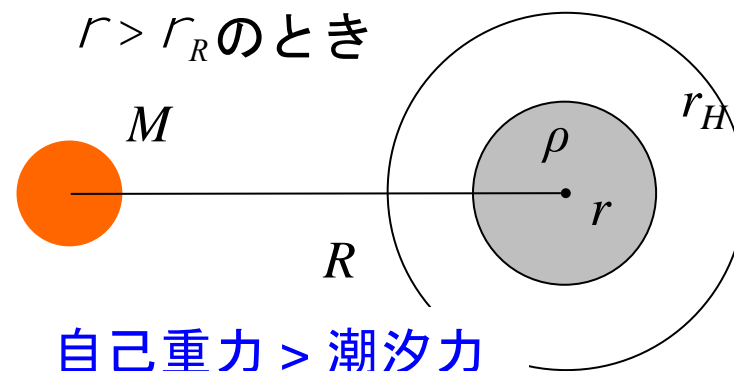
$$r_H = \sqrt[3]{\frac{m_1}{2M}} \quad R = \sqrt[3]{\frac{4\rho/3 \times r r^3}{2M}} \quad R = \sqrt[3]{\frac{r}{r_R}}$$

$r < r_R$ のとき



自己重力 < 潮汐力

$r > r_R$ のとき



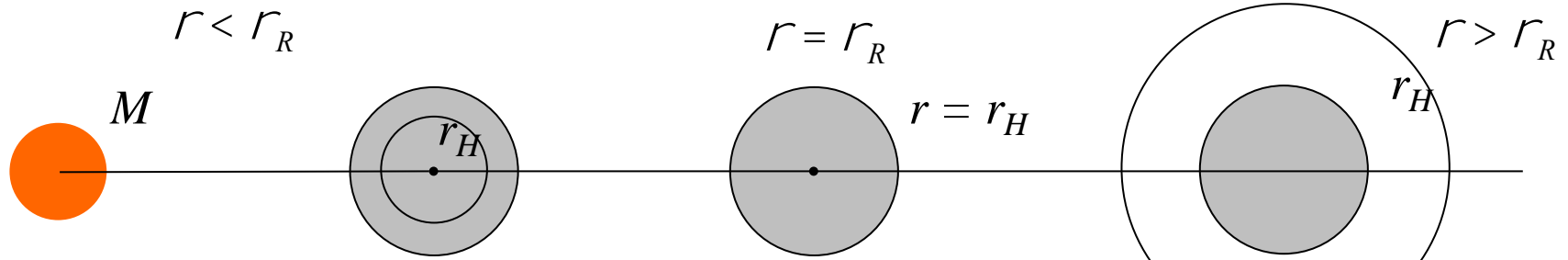
自己重力 > 潮汐力

ロッシュ限界

ρ と r を固定, R を変える $\rightarrow r_R$ が変化する

$$r_R = \frac{2M}{4\rho R^3} \cdot \frac{3}{3}$$

$$r_H = \frac{m_1^{1/3}}{2M^{1/3}} \quad R = \frac{4\rho/3 \times r r^3}{2M} \quad R = \frac{r^{1/3}}{r_R}$$



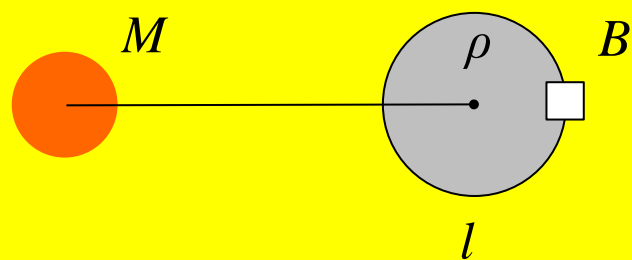
自己重力 < 潮汐力

$$R_R = \frac{2M}{4\rho/3 \times r} \cdot \frac{3}{3}$$

自己重力 > 潮汐力

ロッシュ限界

円盤の重力不安定



$$a = \frac{c_s^2}{l} - \frac{4\rho/3 Gr l^3}{l^2} + 2W_K^2 l$$



$$\frac{a}{l} = \frac{c_s^2}{l^2} - \frac{4\rho/3 Gr l}{l} + 2W_K^2$$

単位質量に働く力
(加速度)

l で割る

$$S = rl$$

$$k = \frac{1}{l}$$

$$w^2 = c_s^2 k^2 - 4\rho/3 GS k + 2W_K^2$$

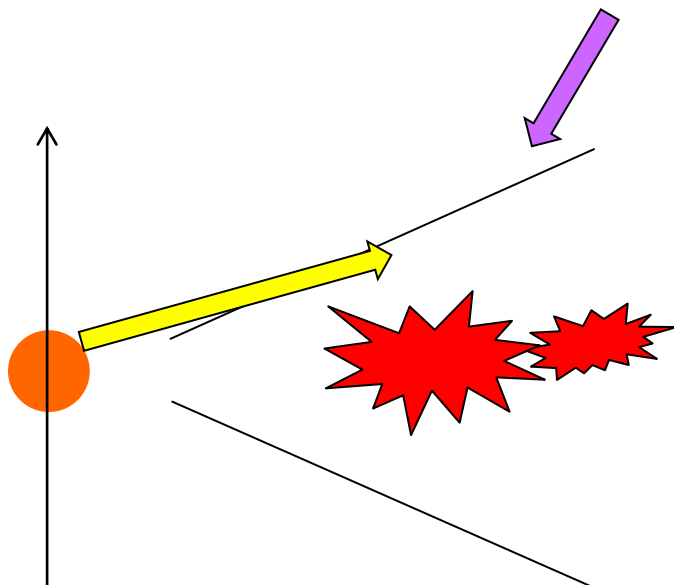
ちゃんとした線形安定性解析によると、

$$w^2 = c_s^2 k^2 - 2\rho GS k + W_K^2$$

$$dr(t) \propto \exp[i(kx - wt)]$$

円盤の温度

- ・熱源
- ・光学的性質



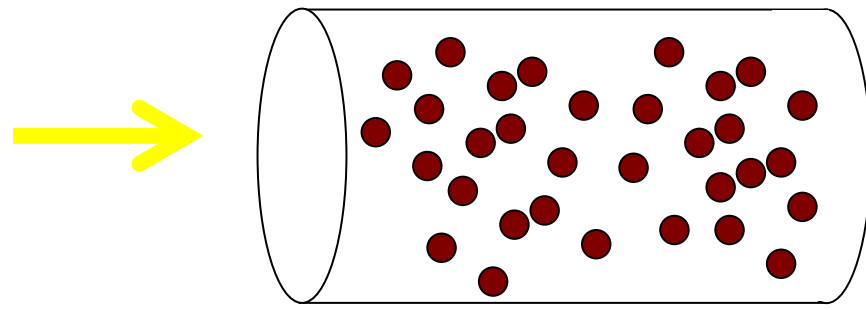
熱源

- ・中心星からの輻射
- ・円盤内で発生する熱
- ・宇宙線

光学的性質

- ・光学的に厚い 不透明
- ・光学的に薄い 透明

光学的厚さ



$x_0 \quad n \quad \sigma \quad x_1$

$$t = \int_{x_0}^{x_1} n S dx = \int_{x_0}^{x_1} r k dx \quad k = \frac{n S}{r} = \frac{S}{m_d}$$

$$I(x) = I(x_0) \exp(-t(x))$$

光学的に薄い円盤の温度

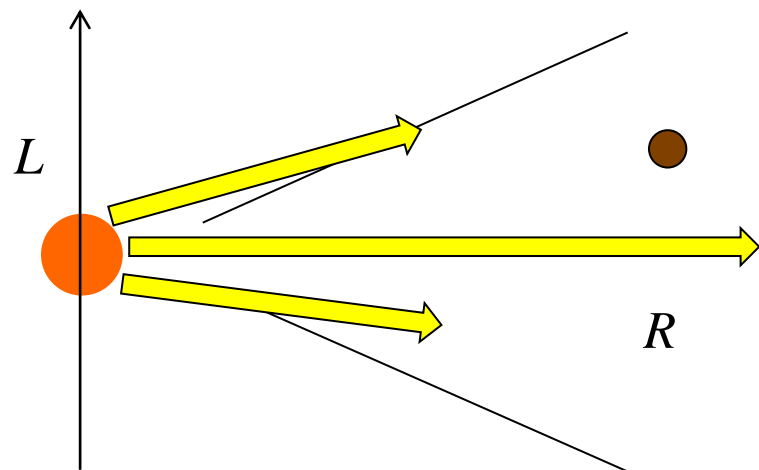
熱源：中心星輻射

固体微粒子：

形状・大きさ = 球, 半径 a

組成 = 氷, シリケイト

黒体



加熱 = 冷却のつり合い

$$\rho a^2 \frac{L}{4\rho R^2} = 4\rho a^2 s T^4$$

$$T = \sqrt[4]{\frac{L}{16\rho s R^2}}$$

$$= 280 \sqrt[4]{\frac{L}{L_{\text{sun}}}} \div \sqrt[4]{\frac{R}{1 \text{ AU}}} \text{ K}$$

円盤の鉛直構造

ガスに働く力のつり合い

r 方向

$$0 = -\frac{1}{r} \frac{dp}{dr} - \frac{GM}{r^2} + rW^2$$

z 方向

$$0 = -\frac{1}{r} \frac{dp}{dz} - \frac{GM}{r^2} \frac{z}{r}$$



$$\frac{1}{r} \frac{dp}{dz} = -W_K^2 z$$

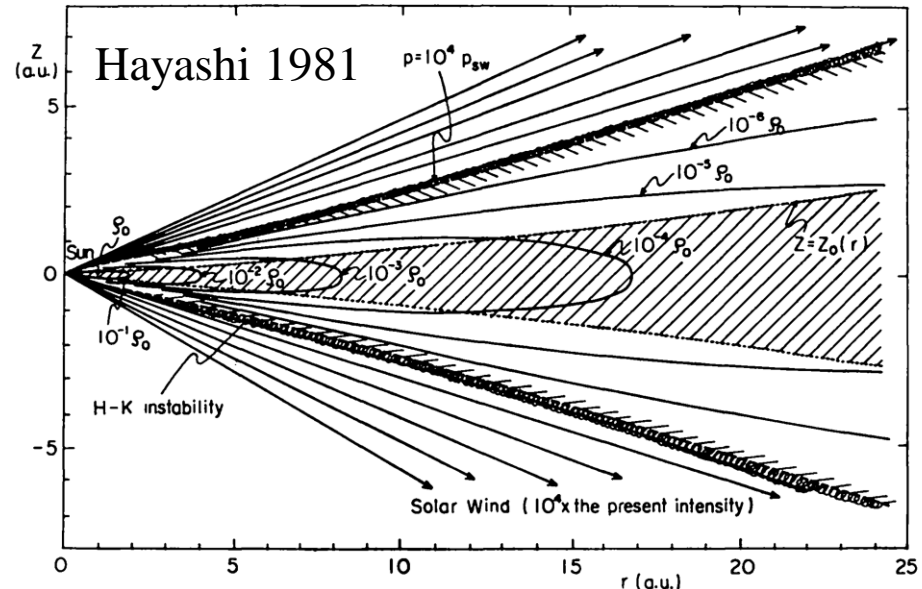


Fig. 2. Structure of the solar nebula and equi-density contours.

$$p(z) = p(0) \exp\left(-\frac{W_K^2 z^2}{2kT/m}\right)$$

$$= p(0) \exp\left(-\frac{z^2}{h^2}\right)$$

$$h = \sqrt{2} \frac{c_s}{W_K} \quad \text{スケールハイト}$$

$$= 0.047 \frac{\mathfrak{C}}{\mathfrak{C} 1 \text{ AU}} \frac{r}{\mathfrak{C} \div \mathfrak{C} 0}^{5/4} \text{ AU} \quad \ll r$$

円盤は幾何学的に薄い

Chiang & Goldreich 1997

2 Layer model

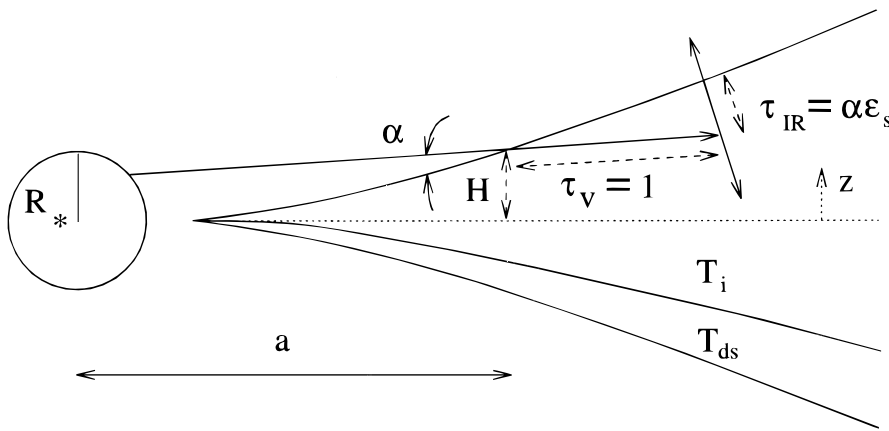


FIG. 3.—Radiative transfer in the passive disk. Stellar radiation strikes the surface at an angle α and is absorbed within visible optical depth unity. Dust particles in this first absorption layer are superheated to a temperature T_{ds} . About half of the emission from the superheated layer emerges as dilute blackbody radiation. The remaining half heats the interior to a temperature T_i .

- ・吸収係数の波長依存性
- ・日向と日影
- ・円盤のフレアアップ

$$T_{ds} = 550 \sqrt{\frac{R}{1 \text{ AU}}}^{-\frac{2}{5}} \text{ K}$$

$$T_i = 150 \sqrt{\frac{R}{1 \text{ AU}}}^{-\frac{3}{7}} \text{ K}$$

放射平衡

$$\int_0^{\infty} k_n J_n dn = \int_0^{\infty} k_n B_n(T) dn$$

吸收

放射

吸收係数

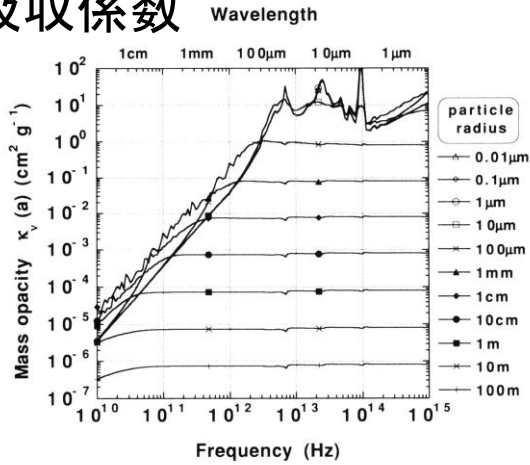
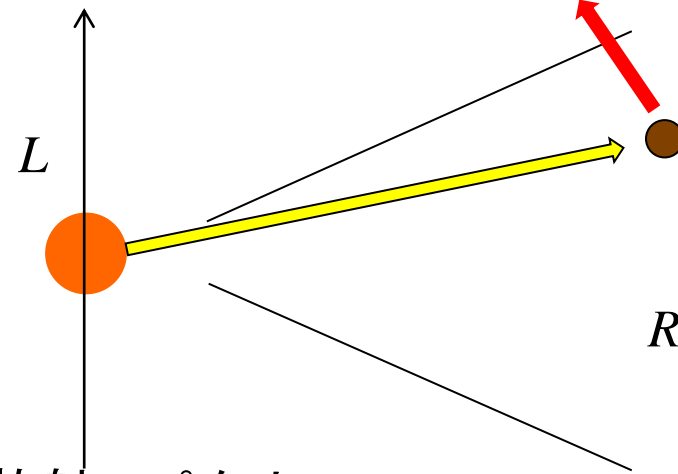
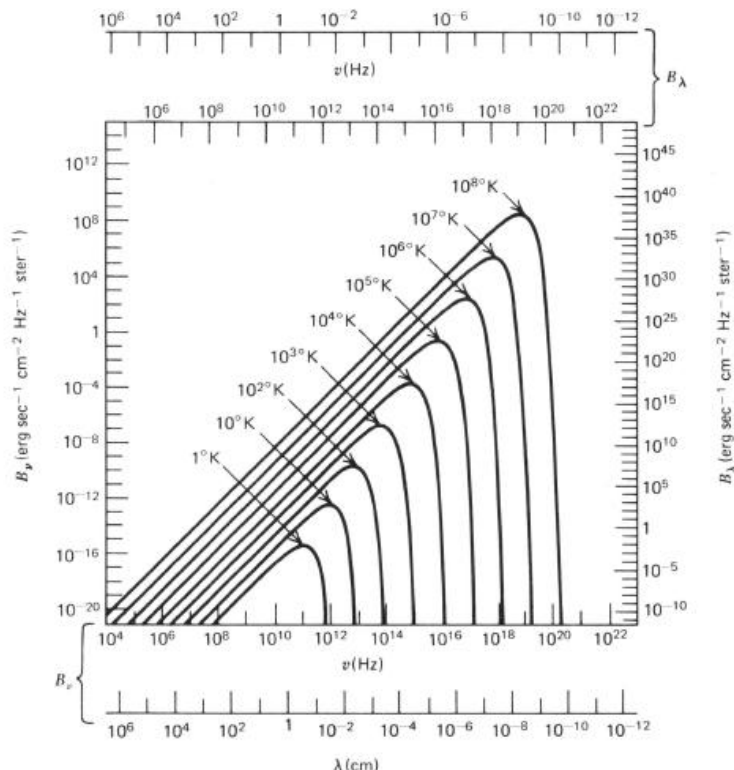


FIG. 4. Mass opacities (in cgs units) of single-sized compact dust particles ($f = 1$) for various radius a ($0.01 \mu\text{m}$ to 100 m) composed of the intimate mixture of silicate and H_2O -ice, where the abundances of dust particles with respect to the H_2 gas are assumed to be solar. Curves for $a \leq 10 \mu\text{m}$ are almost identical at $\nu \leq 10^{12.5} \text{ Hz}$.

Miyake & Nakagawa 1993



黒体放射スペクトル



in “Radiation Processes
in Astrophysics”
Rybicki & Lightman

Figure 1.11 Spectrum of blackbody radiation at various temperatures (taken from Kraus, J. D. 1966, Radio Astronomy, McGraw-Hill Book Company)

固体微粒子の吸収係数

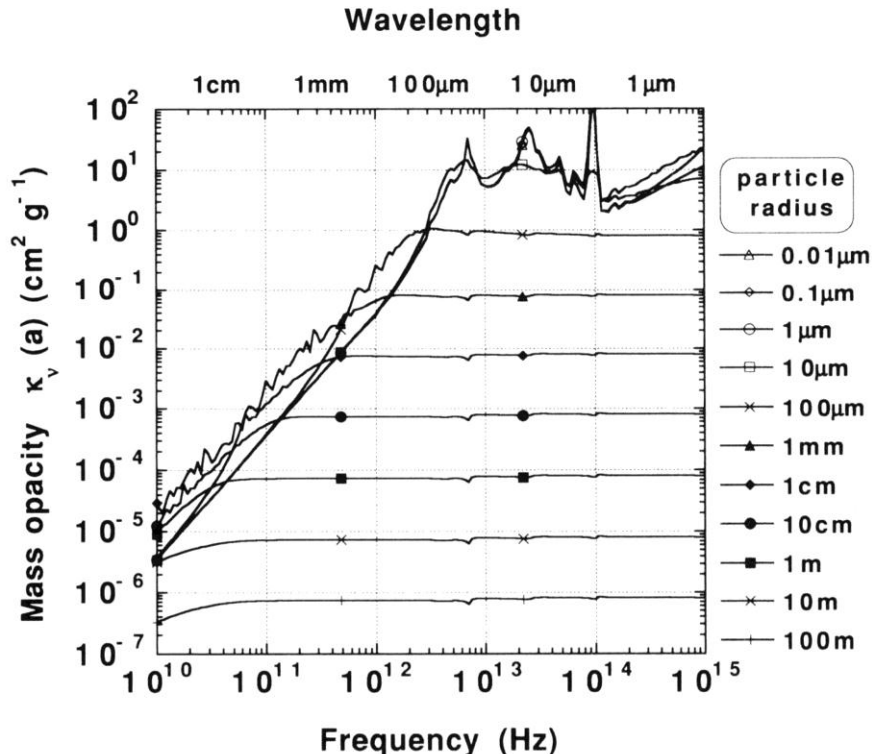


FIG. 4. Mass opacities (in cgs units) of single-sized compact dust particles ($f = 1$) for various radius a ($0.01 \mu\text{m}$ to 100 m) composed of the intimate mixture of silicate and H_2O -ice, where the abundances of dust particles with respect to the H_2 gas are assumed to be solar. Curves for $a \leq 10 \mu\text{m}$ are almost identical at $\nu \leq 10^{12.5} \text{ Hz}$.

Miyake & Nakagawa 1993

黒体放射 スペクトル

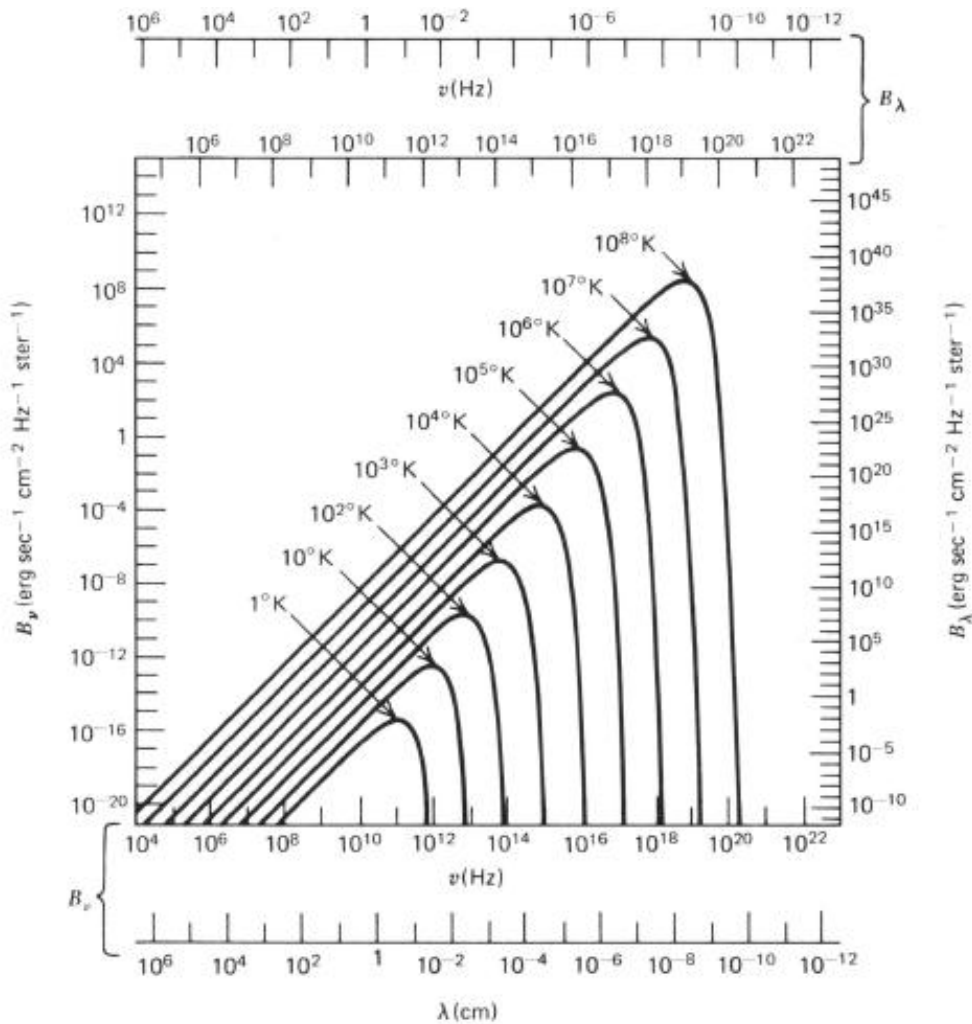


Figure 1.11 Spectrum of blackbody radiation at various temperatures (taken from Kraus, J. D. 1966, Radio Astronomy, McGraw-Hill Book Company)

in “Radiation Processes
in Astrophysics”
Rybicki & Lightman

Effects of scattering and dust grain size on the temperature structure of protoplanetary discs: a three-layer approach

Akio K. Inoue,¹★ Akinori Oka² and Taishi Nakamoto²

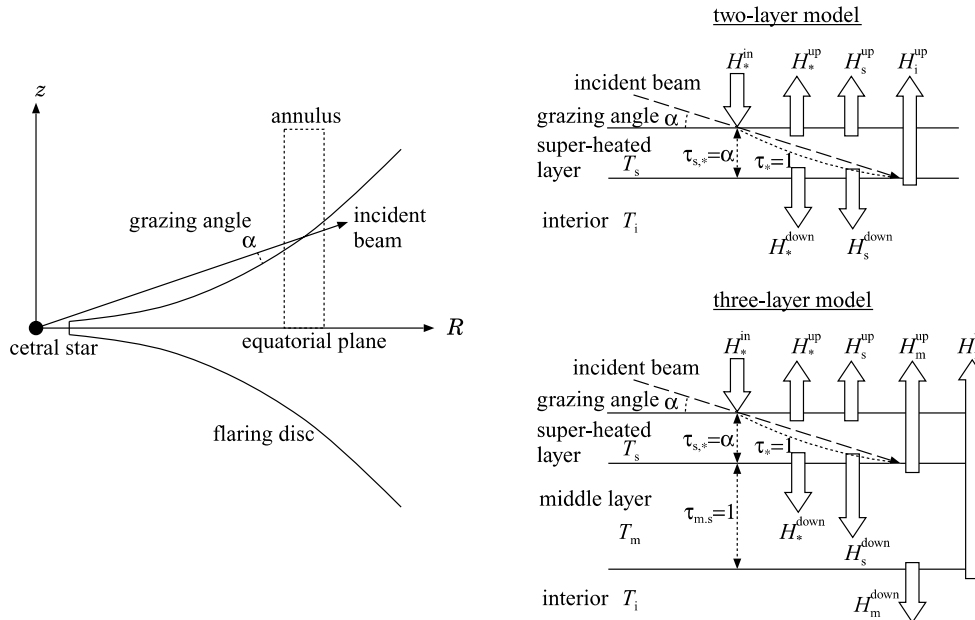


Figure 4. The schematic diagram of the two- and three-layer models. We are considering an annulus clipped from a flaring disc surrounding a young star as shown in the left-hand picture. In the annulus, we consider two or three layers as shown in the right-hand pictures. Each layer is assumed to be isothermal with a temperature T . The fluxes crossing the boundaries of layers are denoted as H^{up} or H^{down} depending on their direction. We set the direction of arrows in the right-hand pictures as the positive direction for the fluxes. The subscript of each quantity indicates the layer associated with the quantity: ‘s’ for the super-heated layer, ‘m’ for the middle layer and ‘i’ for the interior. The quantities with the subscript ‘*’ are associated with the radiation from the central star and H_*^{in} is the stellar flux at the top of the annulus. See also Table 1 for notations.

光学的に厚く、内部熱源がある円盤の温度

$$dw = -\frac{1}{2} \frac{dF}{dr} dr \quad (\text{半分は運動エネルギーに})$$

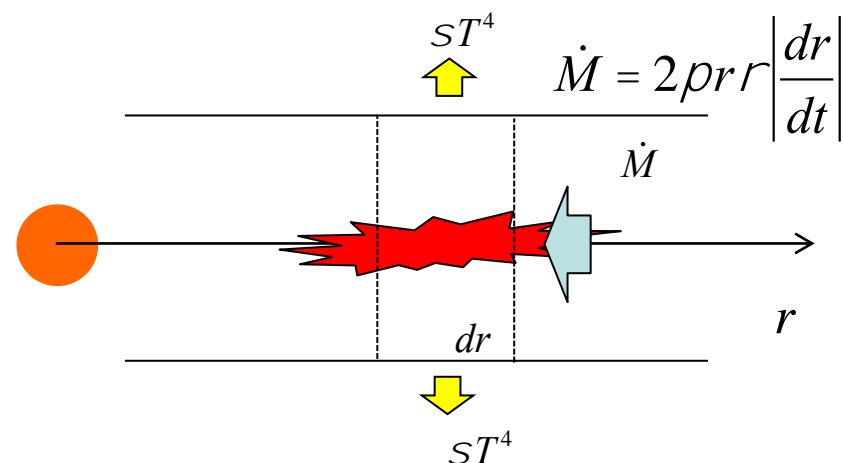
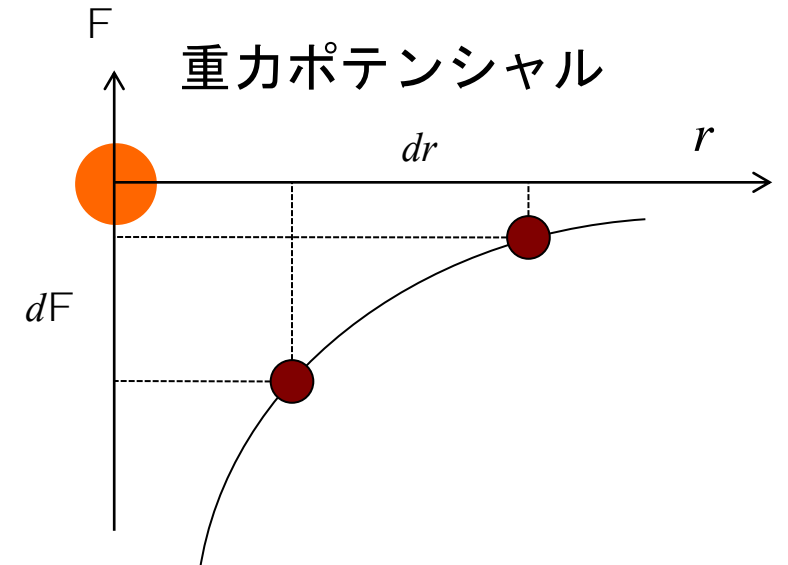
$$= -\frac{1}{2} \frac{d}{dr} \left(\frac{GM}{r} \right) dr = -\frac{1}{2} \frac{GM}{r^2} dr$$

円環 $r \sim r + dr$ での
エネルギーのつり合い

$$2\rho r dr \cdot 2sT^4 = 2\rho r dr \cdot r \frac{1}{2} \frac{GM}{r^2} \left| \frac{dr}{dt} \right|$$

$$2sT_s^4 = \frac{GMM'}{4\rho r^3} \times 3 \quad (\text{移流の効果})$$

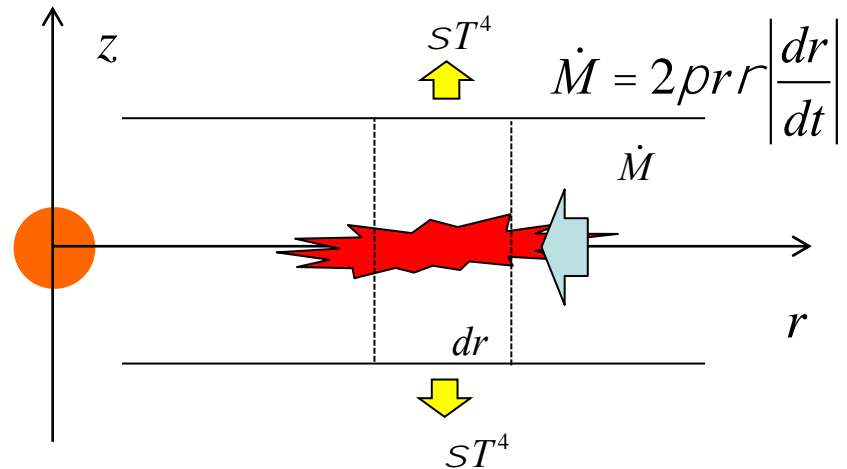
$$T_s = \frac{3GM}{8\rho s r^3}^{1/4} \quad \text{円盤表面温度}$$



光学的に厚く、内部熱源がある円盤の温度

z 方向輻射エネルギー フラックス
(拡散近似)

$$F(z) = -\frac{4S}{3rk} \frac{dT^4}{dz}$$



熱源は $z = 0$ に限定 & $z > 0$ を考える

$$\int_0^h F(z) dz = \int_0^h -\frac{4S}{3rk} \frac{dT^4}{dz} dz$$

$$\text{左辺} = \int_{t/2}^0 F dt = F \times \frac{t}{2} = ST_s^4 \times \frac{t}{2}$$

$$\text{右辺} = \int_{t/2}^0 \frac{4S}{3} \frac{dT^4}{dt} dt$$

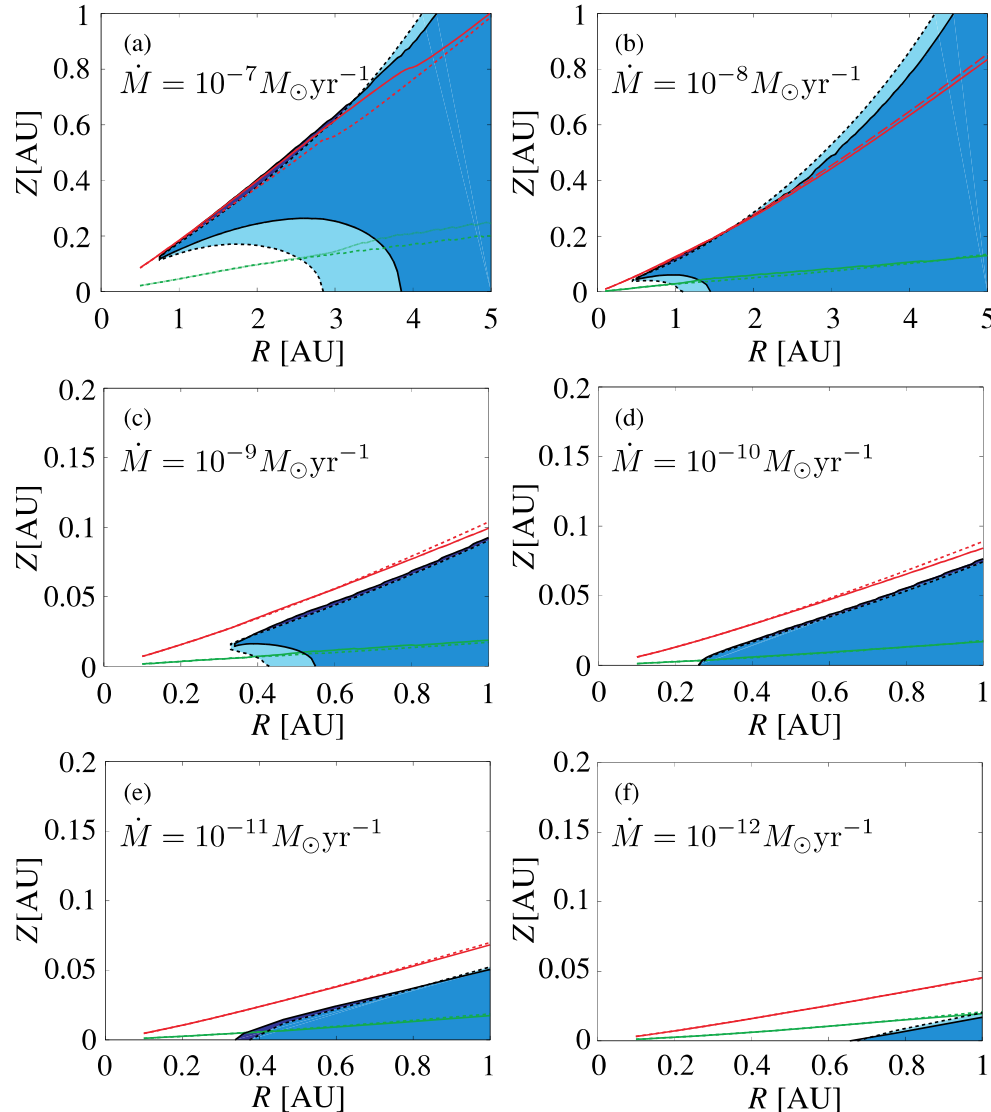
$$= \frac{4S}{3} (T(0)^4 - T_s^4)$$

ゆえに

$$T(0) = T_s \left(1 + \frac{3t_0^{1/4}}{8} \right)$$

$$t = \int_{-h}^h rk dz$$

中心星輻射 + 円盤内熱源



Z 方向の輻射輸送は
正確に計算
(拡散近似は使わず)

青色領域 : $T < 170\text{K}$

円盤の温度の影響

組成 :

- ・シリケイト成分
 - ・氷 (水, CO, NH₃, ...)
 - ・金属Fe, Ni
 - ・有機物
- $T \sim 170\text{ K}$ で固化/蒸発
スノーライン

力学 :

- ・ガスの流れ, 構造
- ・固体微粒子の移動
- ・惑星の移動

円盤内の質量の流れ

質量保存の式

$$\frac{\partial S}{\partial t} + \frac{1}{R} \frac{\partial}{\partial R} \left(R S v_R \right) = S(R, t) \quad S = \int r dz \quad \text{面密度}$$

R方向のつり合い

$$0 = -\frac{GM}{R^2} + \frac{j^2}{R^3} \quad j = R^2 W$$

φ 方向の運動方程式/

角運動量保存の式

$$\frac{\partial(Sj)}{\partial t} + \frac{1}{R} \frac{\partial}{\partial R} \left(\dot{S}v_R j - \mathbf{T} \right) = S(R, t) j_*$$

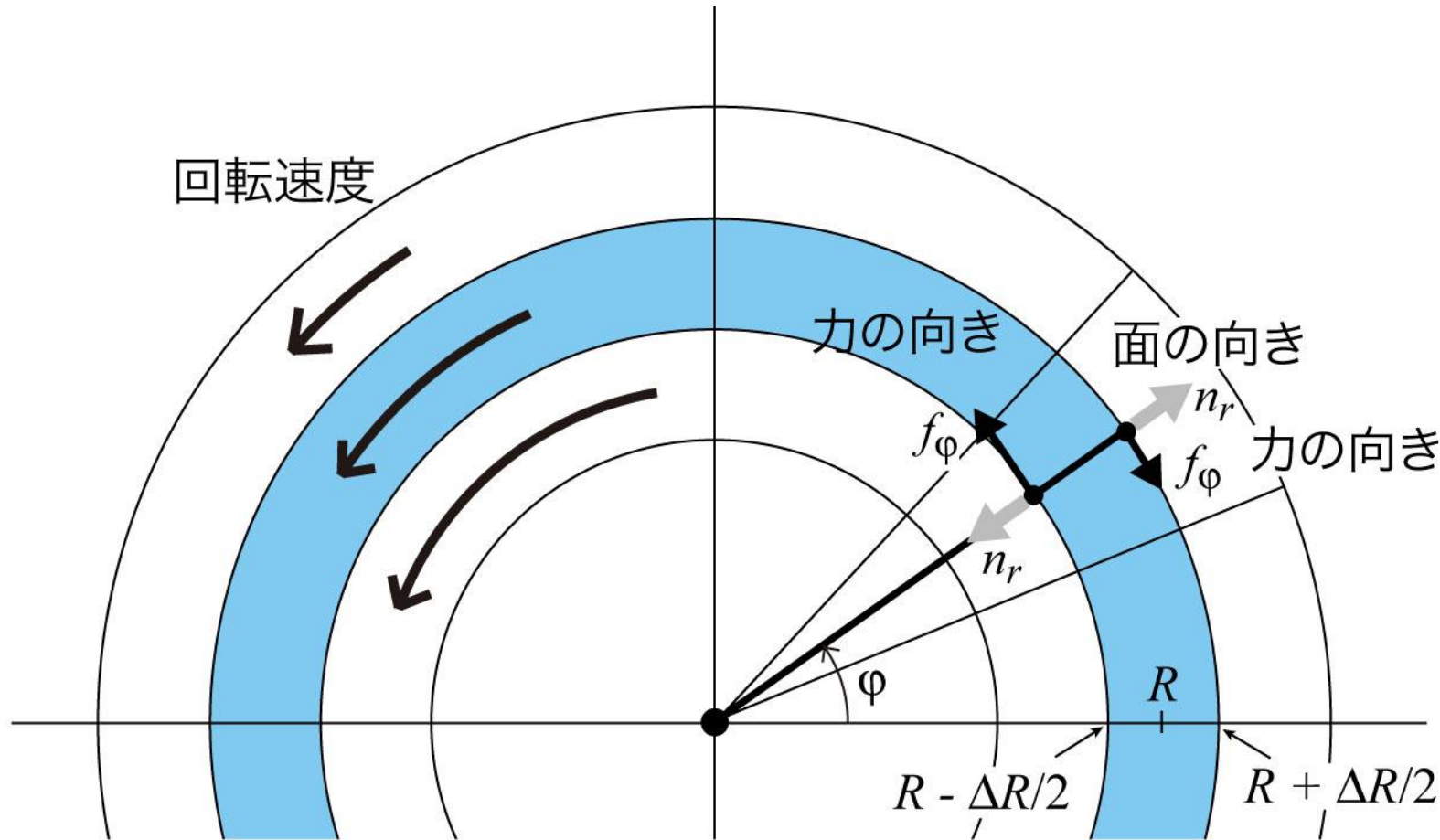
↑
トルク

エネルギーの式

状態方程式

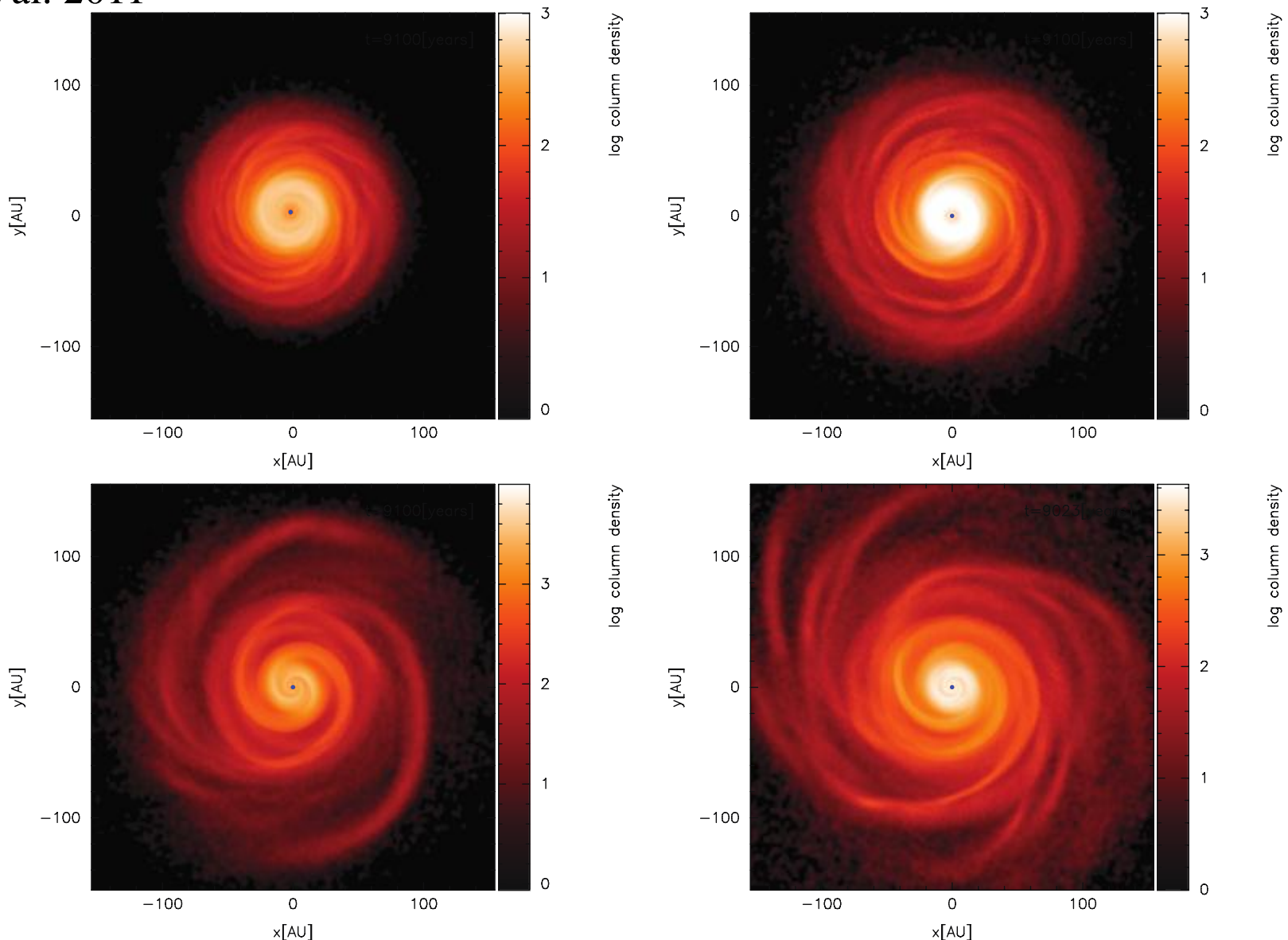
円盤の力学的進化

$$\text{粘性トルク } T = Rf_j = nSR^2 \frac{dW}{dR}$$



トルクの源は？

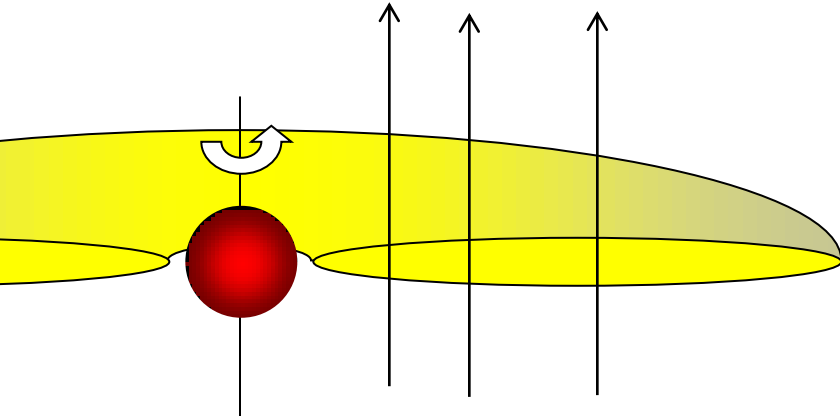
- ・MRI乱流
- ・自己重力



• 1. Images showing the surface density structure of Simulations 1 (top left-hand panel), 2 (top right-hand panel), 3 (bottom right-hand panel) after 27 ORPs. The stellar mass in each case is $1 M_{\odot}$, and the initial disc masses of 0.2, 0.5, 1 and $3.5 M_{\odot}$ are shown in each figure and it is clear that the more massive discs exhibit higher amplitude spiral structures, in particular the *m*

磁気回転不安定 (Magneto-Rotational Instability; MRI)

Hawley & Balbus 1991



円盤ガスが弱く電離
している場合

磁気流体

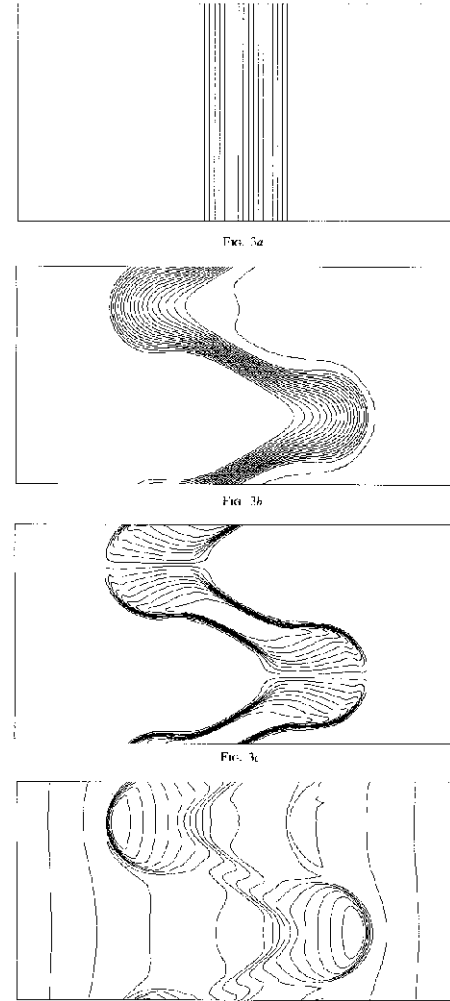


FIG. 3. Contour plots of (a) the *initial* poloidal magnetic field lines, and (b) the poloidal magnetic field lines, (c) toroidal field, and (d) angular momentum at 3.3 orbits in the $P_2 = 1000$, $\alpha = 1$ high-resolution simulation (Model 2b). There are 20 linearly spaced contours. The angular momentum values run from 9.91 to 10.08, the Keplerian value of the angular momentum at the center of the grid is 10. The toroidal field has a maximum energy density of 2×10^{-3} .

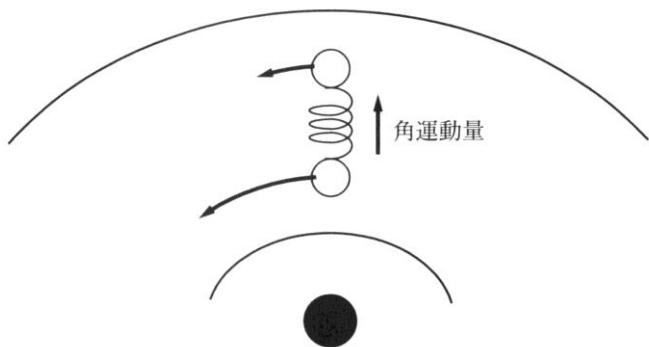


図 8.3 重力回転系における不安定性。2つの粒子を弱いばねで結ぶ運動量が輸送されて粒子間の距離はしだいに離れていく

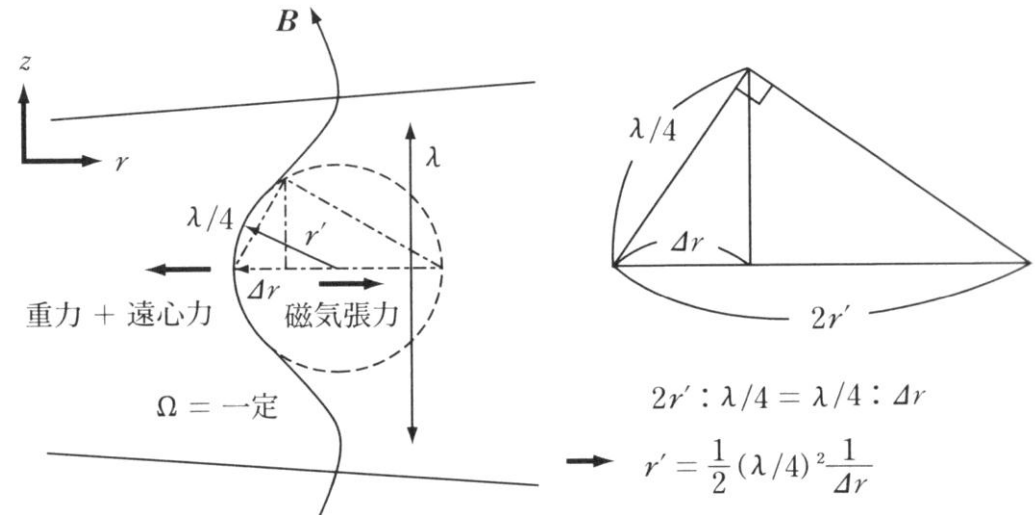


図 8.4 磁気回転不安定性が成長するための条件。流体要素を Δr だけ変位させたときの重力+遠心力が磁気張力より大きい場合に不安定になる

$$\text{遠心力} = (r - \Delta r) r \dot{\theta}^2$$

$$\text{重力} = -\frac{GM}{r^2} \left(1 + 2\frac{\Delta r}{r}\right)$$

$$\text{遠心力+重力} = -3r\dot{\theta}^2\Delta r$$

$$\text{磁気張力} = \frac{B^2}{m_0 r'} = \frac{2B^2 \Delta r}{m_0 (\lambda/4)^2}$$

松元亮治(1999)

磁気張力 - (遠心力+重力)

$$= \left[\frac{2B^2}{m_0 (\lambda/4)^2} - 3r\dot{\theta}^2 \right] \Delta r < 0 \quad : \text{不安定の条件}$$

$$\lambda > \lambda_{\text{crit}} = \sqrt{\frac{32}{3}} \frac{B^2}{m_0 r} \cdot \frac{1}{\dot{\theta}}$$

波長 $\lambda > \lambda_{\text{crit}}$ の波に対して不安定

トルク $\mathbf{T} = Rf_j = R \left\langle dv_R dv_j - \frac{B_r B_j}{4\rho r} \right\rangle_r$

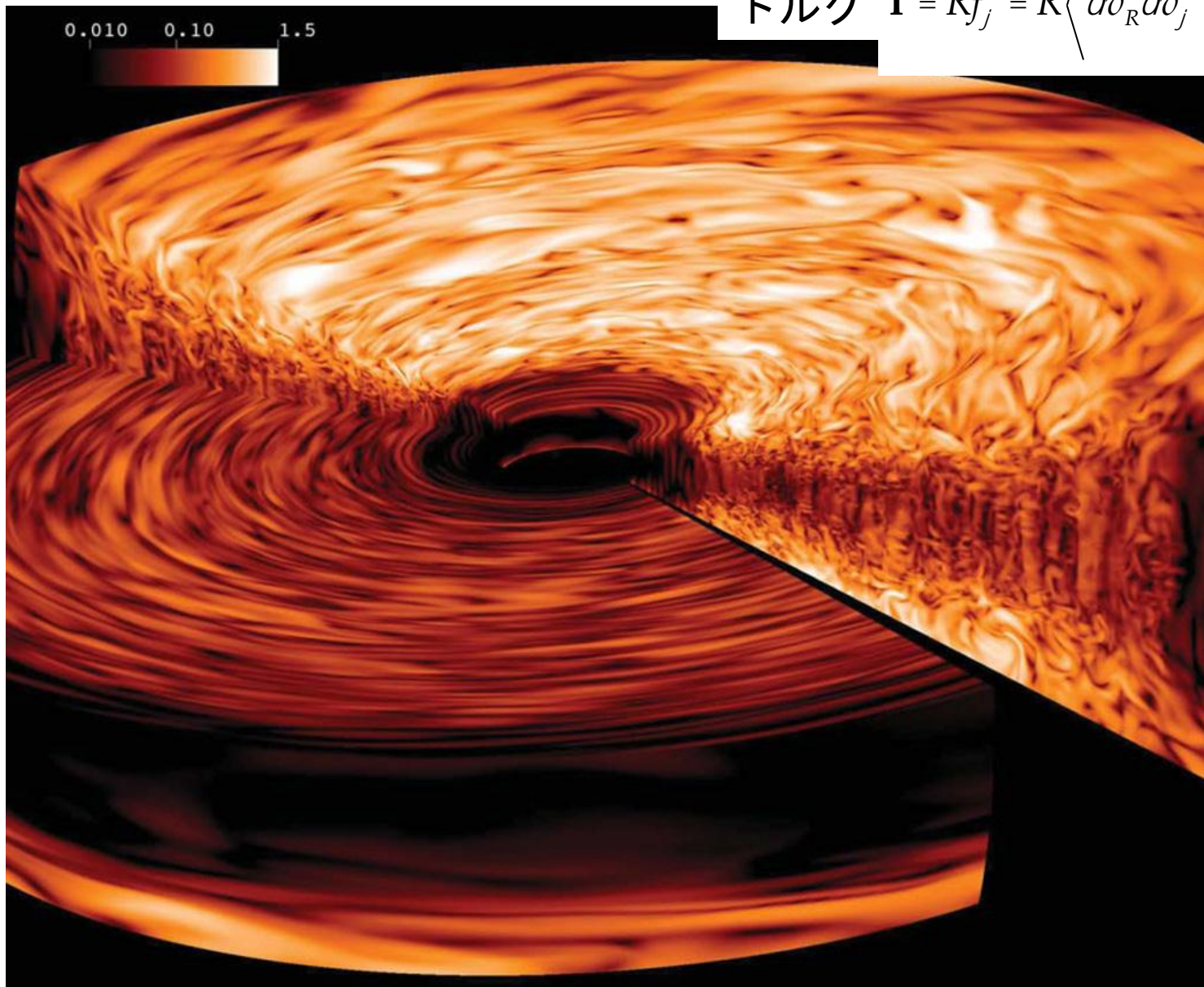


Figure 7. 3D picture of turbulent rms velocity at 750 inner orbits for model BO. The white regions in the corona present super-sonic turbulence.

Turbulence and Accretion in 3D Global MHD Simulations of Stratified Protoplanetary Disk

Dead Zone

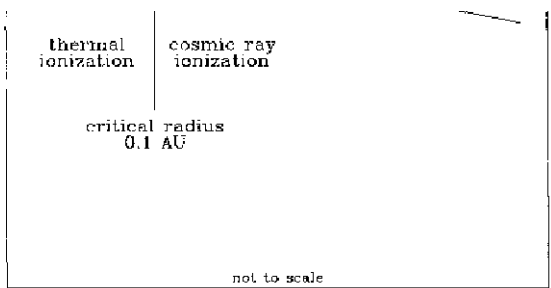
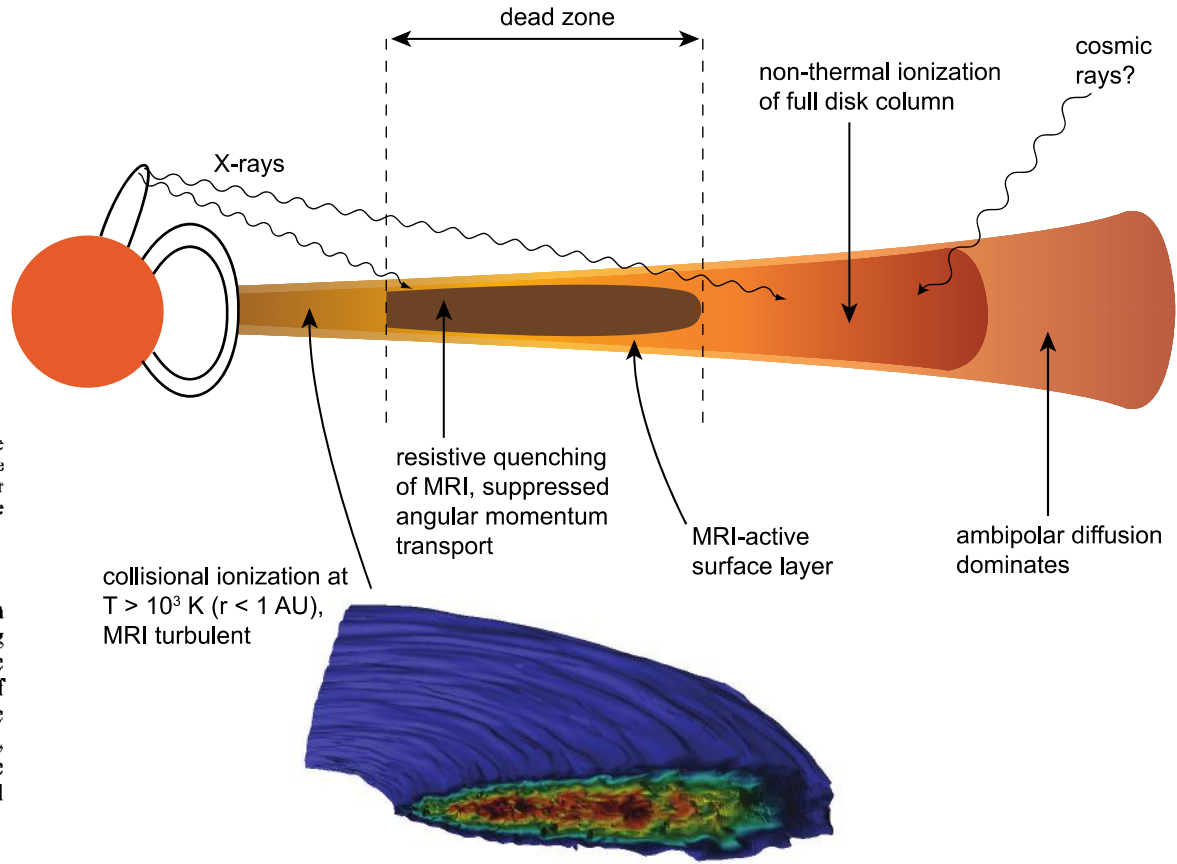


FIG. 1.—Sketch showing the key features of a layered accretion disk. Inside ≈ 0.1 AU, where $T \approx 10^3$ K, collisional ionization is sufficient to couple the magnetic field to the gas. Outside this critical radius cosmic rays ionize a layer of thickness $\approx 100 \text{ g cm}^{-2}$ on either side of the disk. Sandwiched between these active layers is a dead zone where no accretion occurs.

A graphical summary of the structure of magnetically driven low-ionization disks is given in Figure 1. From the accreting star out to the critical radius R_c , where $T < 10^3$ K, the entire disk is coupled to the field because collisional ionization of alkali metals is effective. At larger radii the disk has an active layer near the surface where cosmic-ray ionization is effective, and a dead zone near the midplane. The dead zone will come into thermal equilibrium with the base of the active layer (and



Armitage 2011

Gammie 1996

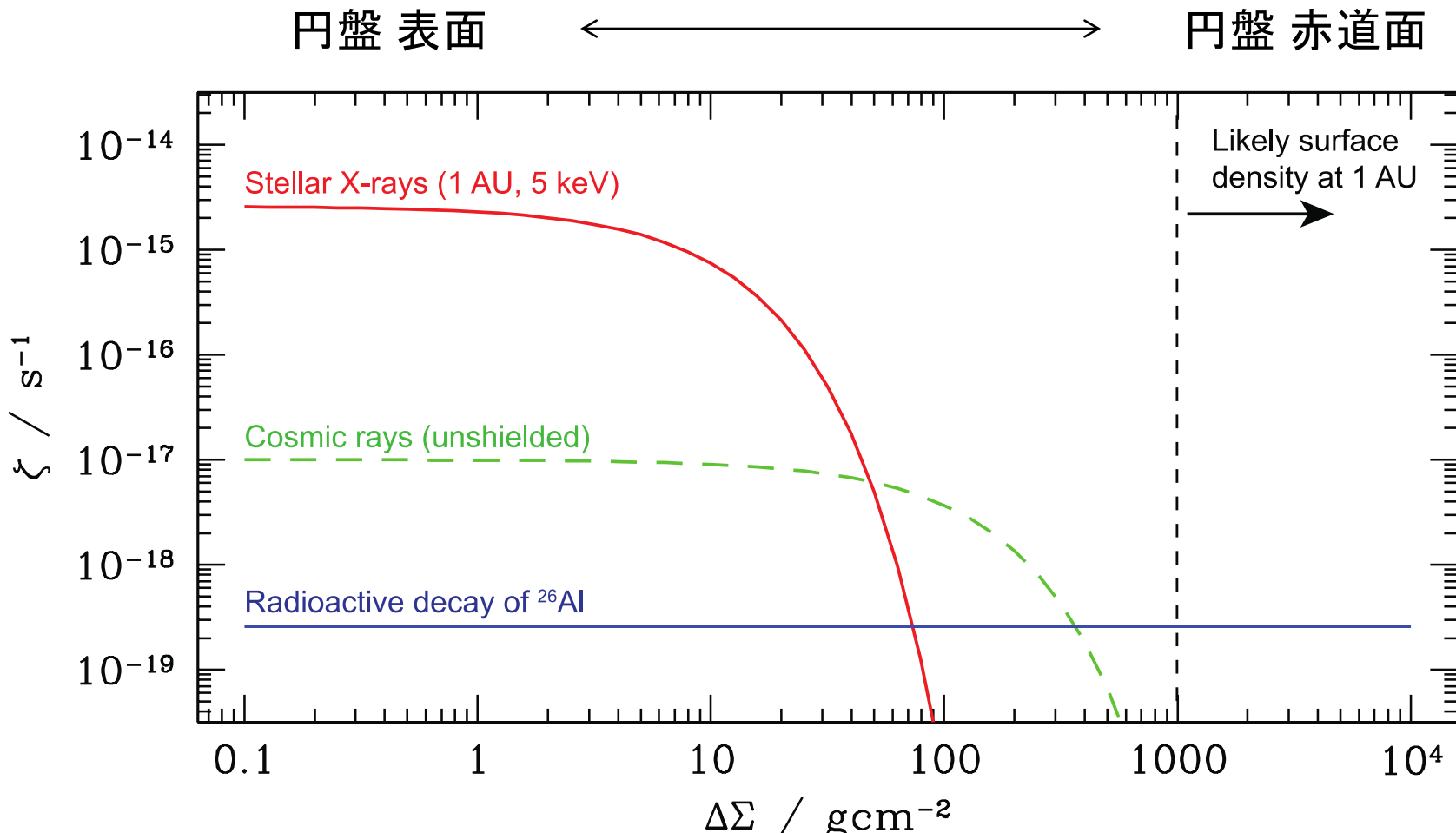


Figure 6: The dependence of the ionization rate ζ on the column density $\Delta\Sigma$, measured from the disk surface. Contributions from the three three main sources of non-thermal ionization are shown: (a) stellar X-rays, evaluated at 1 AU (as a function of radius, $\zeta \propto r^{-2}$) using the Turner & Sano

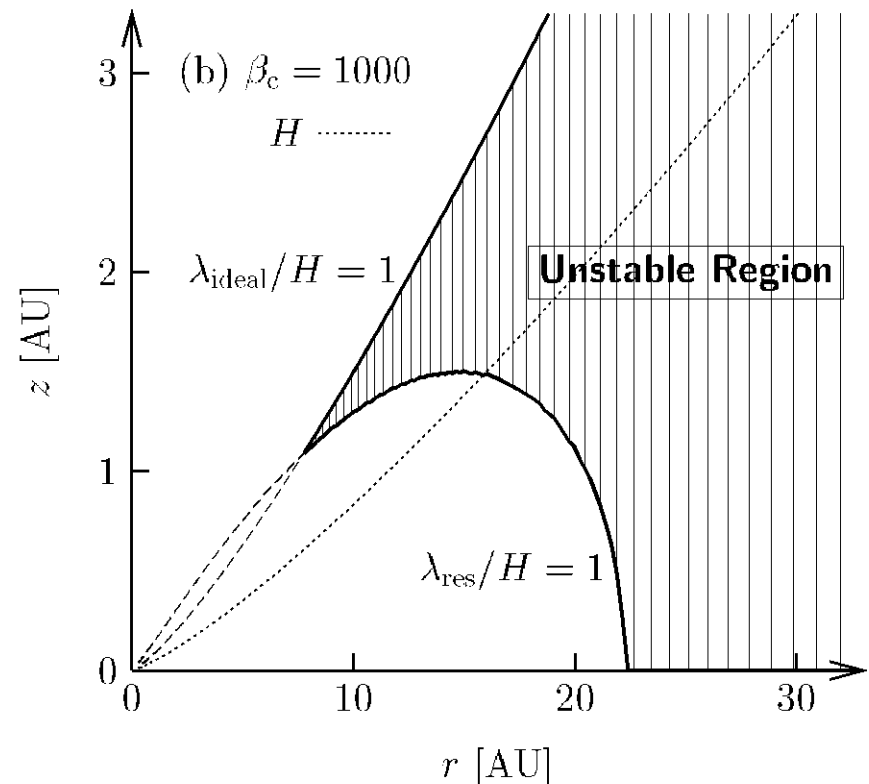
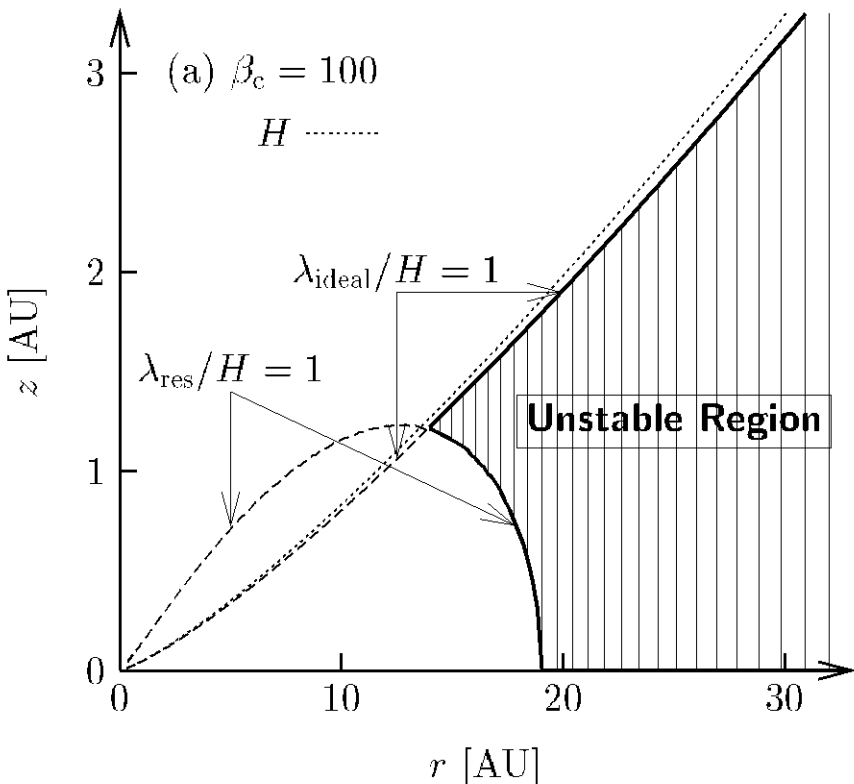
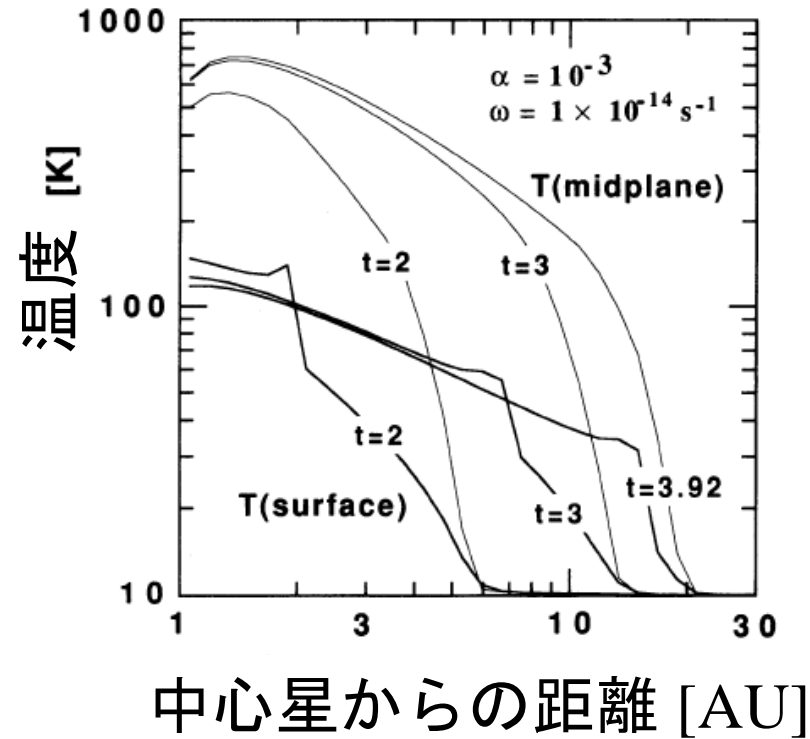
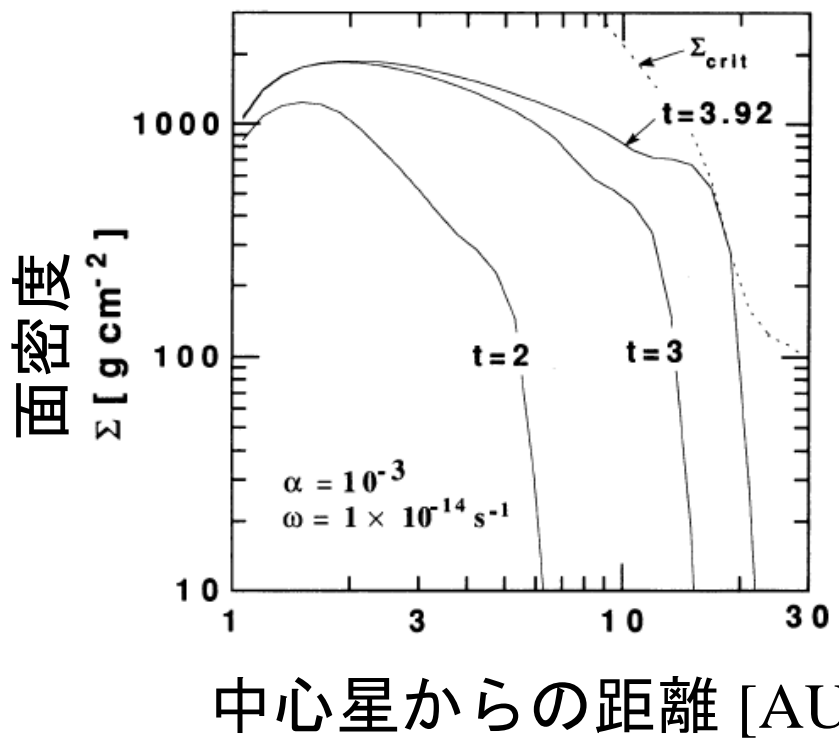


FIG. 7. Unstable regions (striped) for the cases of (a) the plasma beta at the midplane $\beta_c \neq 100$ and (b) $\beta_c \neq 1000$ for the fiducial model (same as in Fig. 1). The dotted curve denotes the scale height of the disk, $z \neq H(r)$. In the region above the curve $\lambda_{\text{ideal}}/H \neq 1$, the instability does not effectively work because the wavelengths of the unstable modes are larger than the scale height of the disk. The region below the curve $\lambda_{\text{res}}/H \neq 1$ is stable because the magnetic dissipation is effective and corresponds to Gammie's (1996) "dead zone".

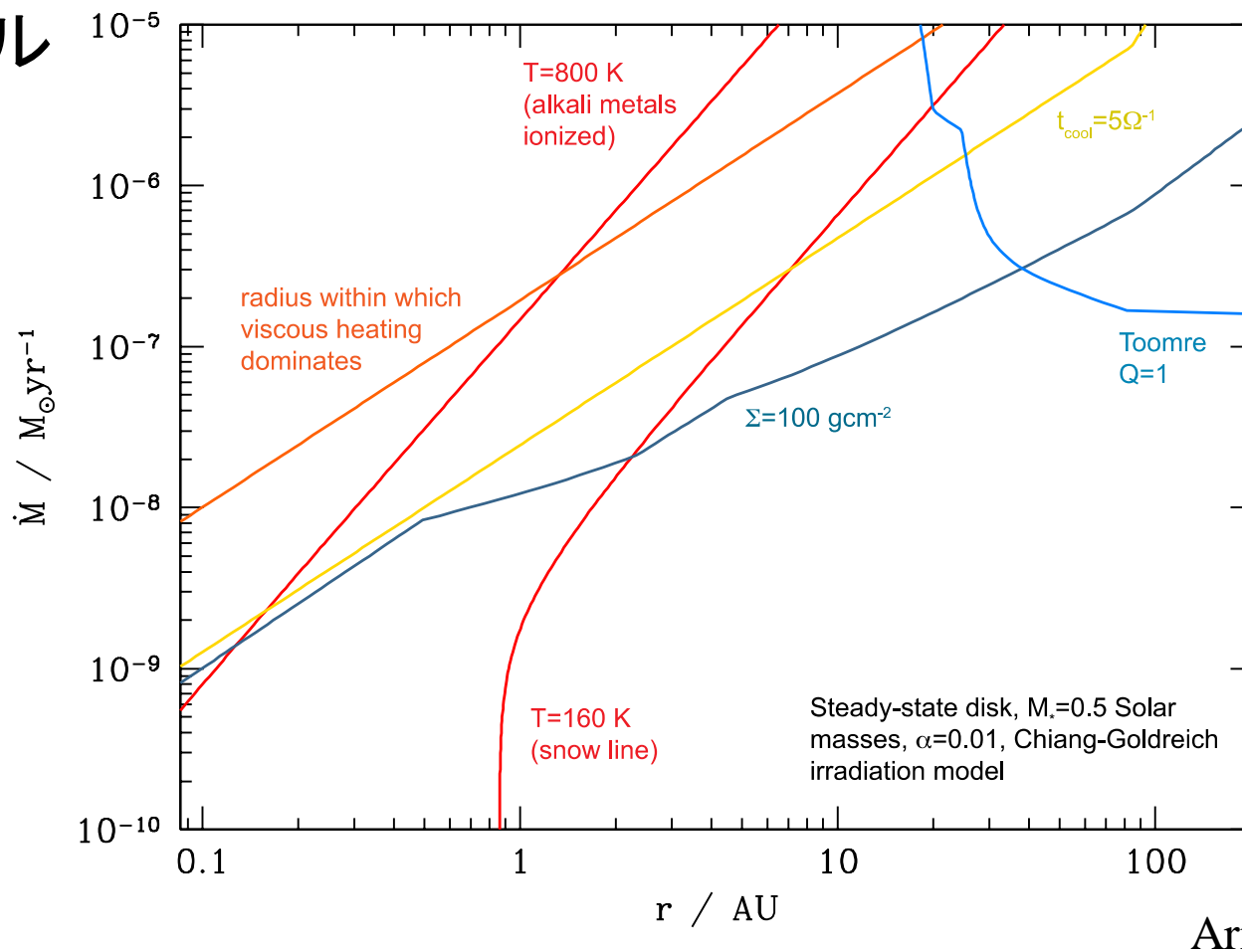
円盤進化モデルの一例

円盤の質量分布・温度分布



Nakamoto & Nakagawa 1994

円盤モデル 計算の例



Armitage 2011

Figure 2: Illustration of how critical disk radii, delimiting different physical regimes relevant to angular momentum transport and planet formation, scale with accretion rate M . Temperatures are mid-plane values, the cooling time scale is defined as $t_{\text{cool}} = \Sigma c_s^2 / 2\sigma T_{\text{eff}}^4$, and the Toomre Q parameter $Q = c_s \Omega_K / \pi G \Sigma$. The plot is based upon a one-zone vertical model (calculated as described, e.g., by Frank, King & Raine 2002) of a steady-state α disk around a $0.5 M_{\odot}$ star, with $\alpha = 10^{-2}$. The opacity includes contributions from water ice, amorphous carbon, silicates and graphite (Z. Zhu, private communication). The calculation is approximate: the radial dependence of stellar irradiation is assumed to follow the Chiang & Goldreich (1997) form, independent of both time and disk accretion rate.

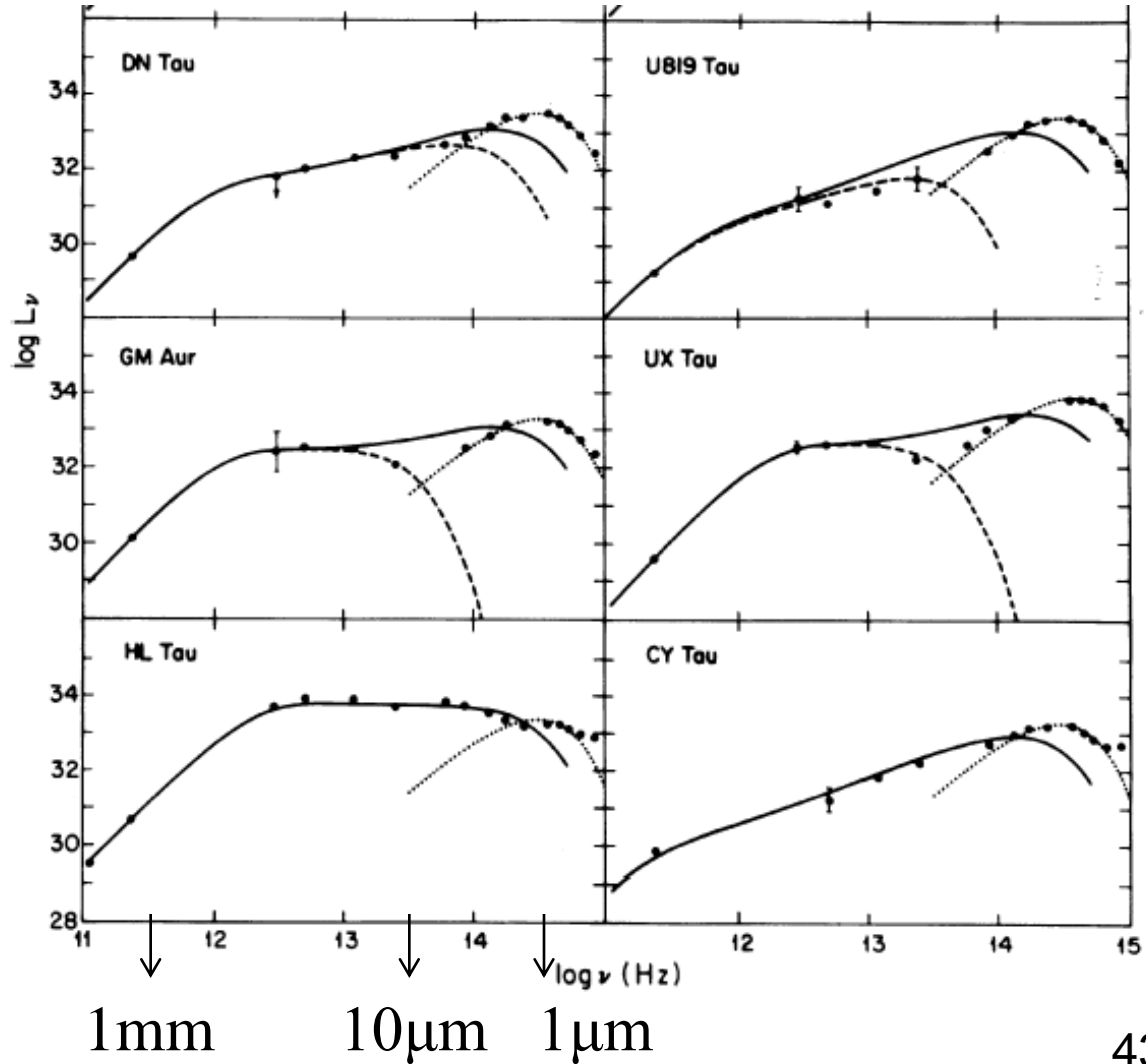
T タウリ型星 (T Tauri Stars) のスペクトル

$$L_n = 4\rho \cos q \int_0^\infty n B_n(T)(1 - e^{-t_n}) 2\rho R dR$$

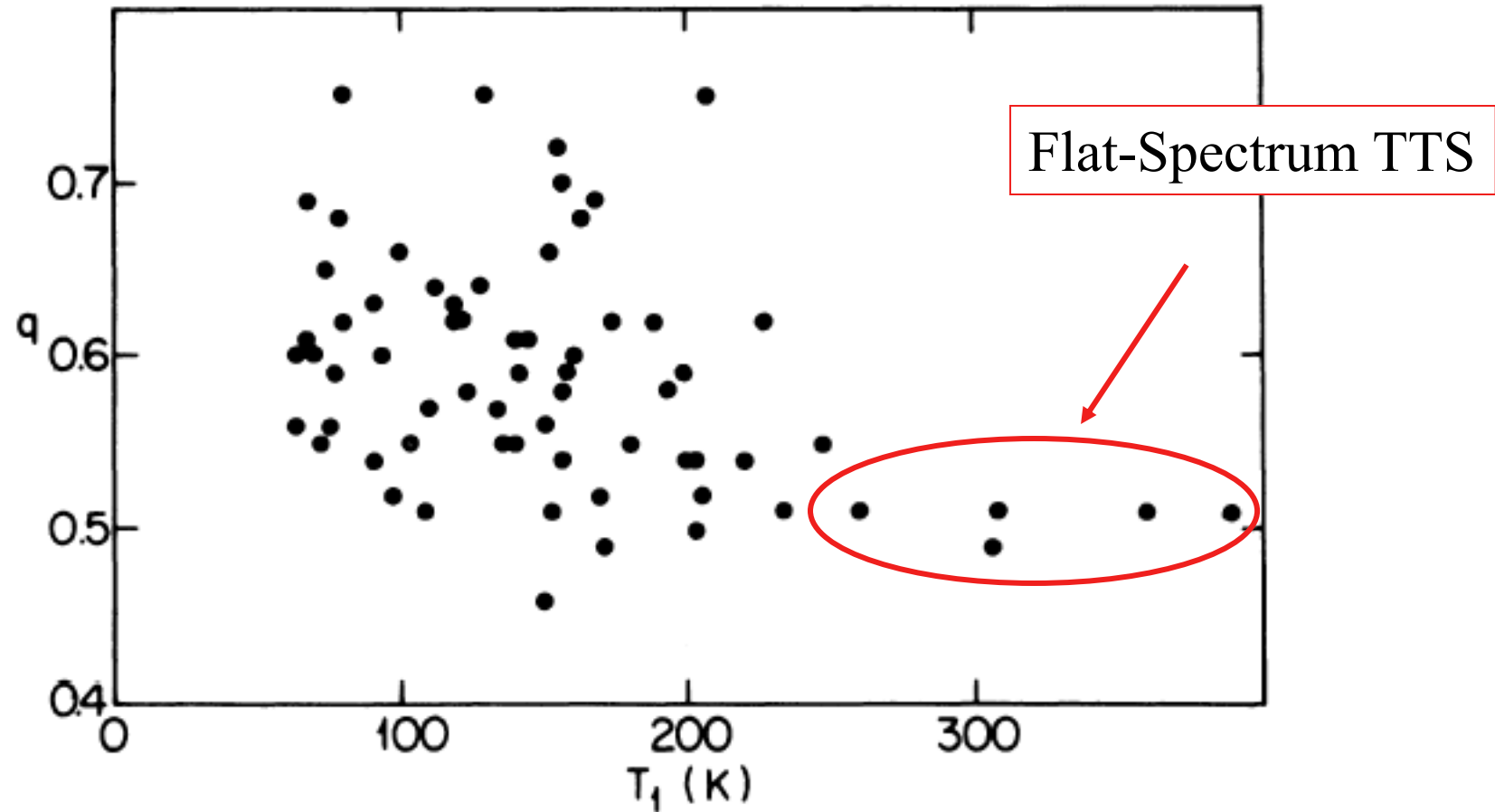
Beckwith et al. 1990, AJ 99, 924

$$S(R) = S_1 \frac{R}{1\text{AU}}^{-p}$$

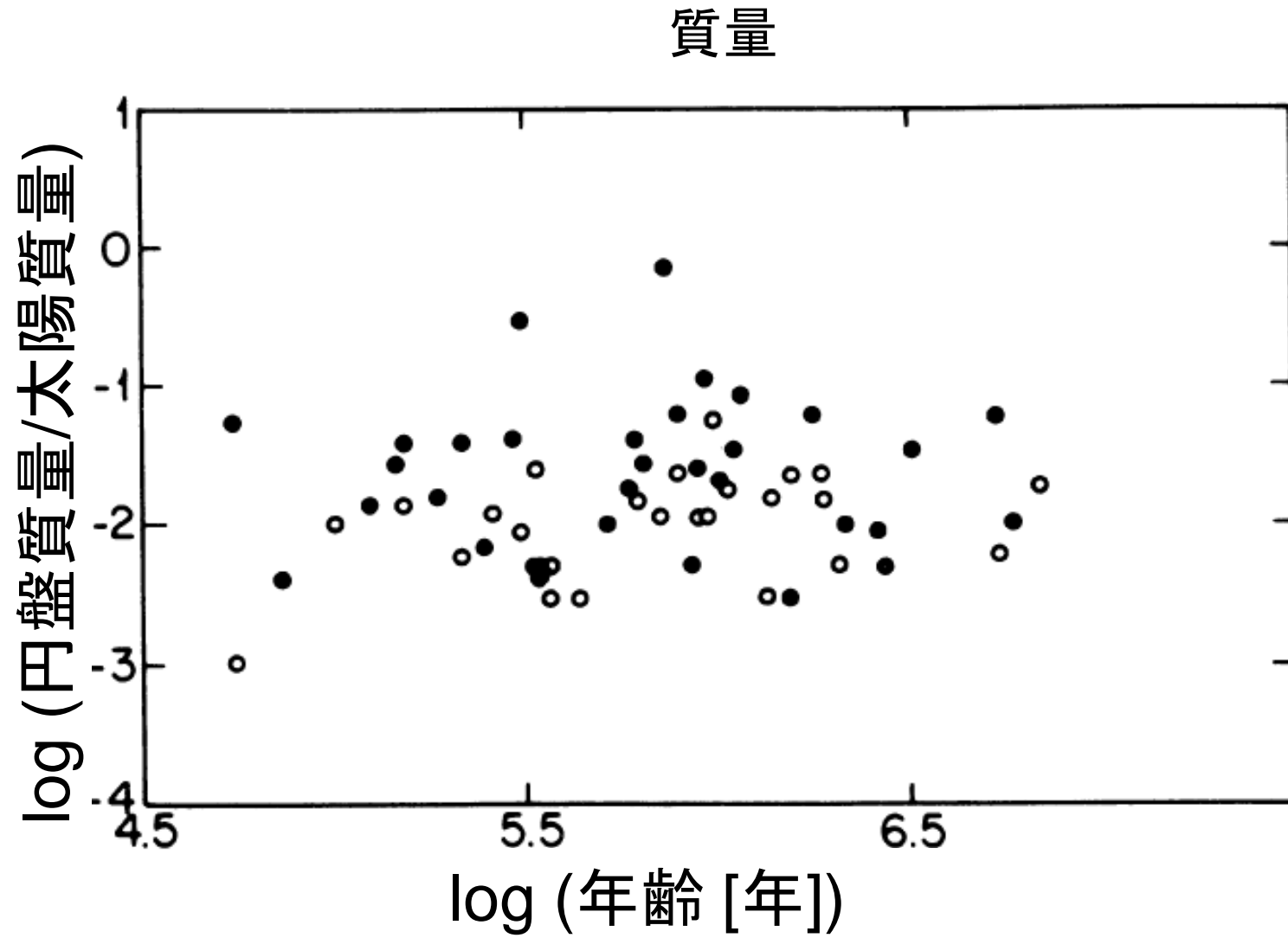
$$T(R) = T_1 \frac{R}{1\text{AU}}^{-q}$$



Tタウリ型星(TTS)の円盤の表面温度分布



円盤の観測例



円盤の観測

Sicilia-Aguilar et al. 2006b

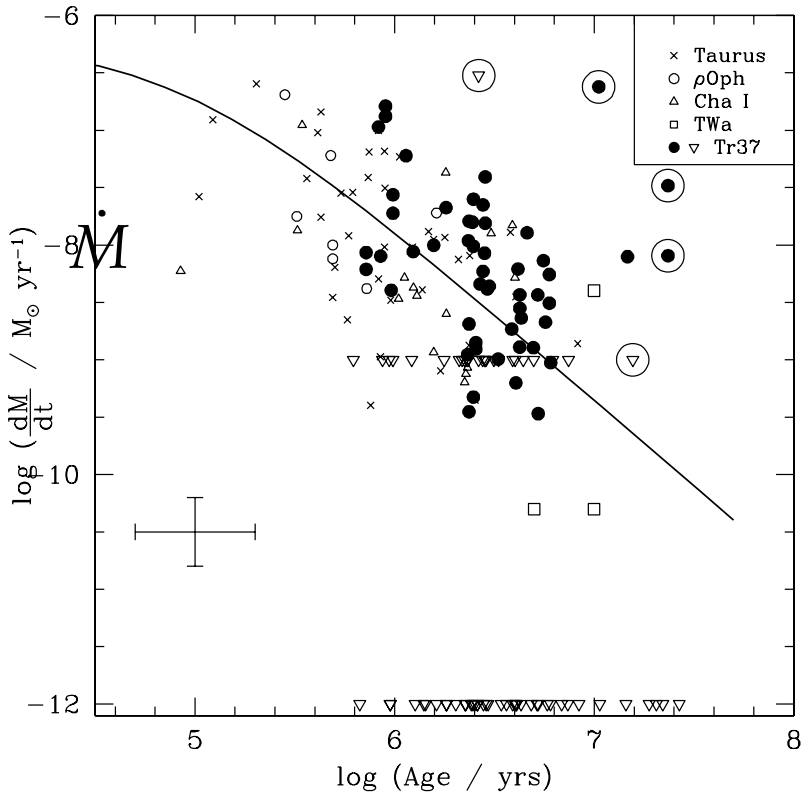


FIG. 11.—Accretion rate vs. age in Tr 37. Filled circles represent stars with accretion rates derived from the U band (see Paper I and Paper II for a discussion about the accretion rate estimates). Triangles represent upper limits to the accretion based on the presence of broad $H\alpha$ emission ($10^{-9} M_\odot \text{ yr}^{-1}$) in stars for which we did not find any U excess (U -band observations were complete to approximately the U photospheric emission of a K6 star) and the lack of broad components in stars with no U excess ($10^{-12} M_\odot \text{ yr}^{-1}$). For comparison, we include data from other regions and the model for the evolution of a viscous disk (Hartmann et al. 1998; Muzerolle et al. 2000). The average accretion rate in Tr 37 (including the upper limits but excluding the G-type stars, marked here with open circles) is shown with error bars.

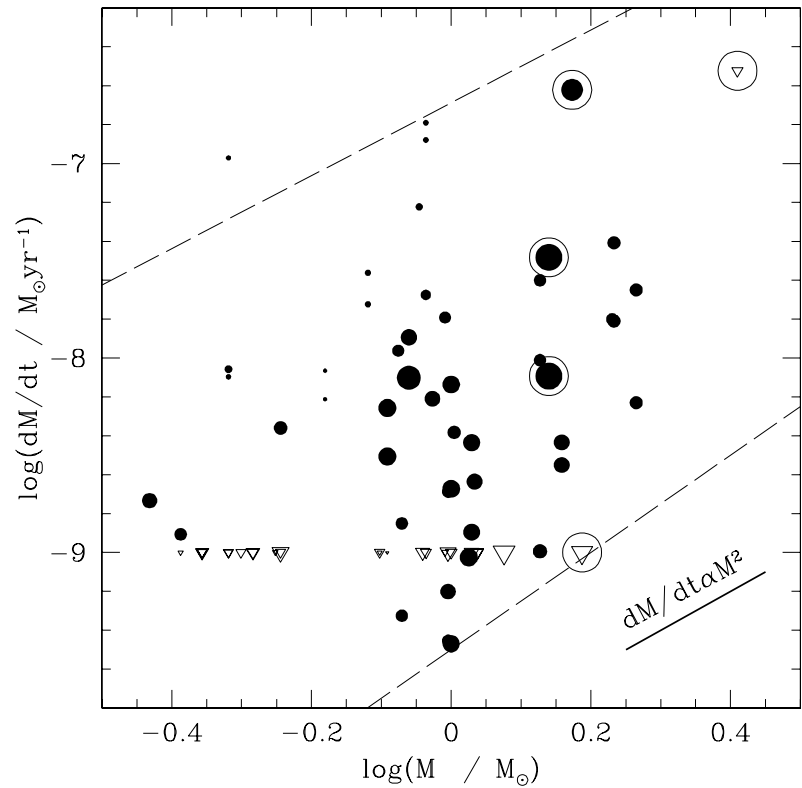


FIG. 12.—Accretion rate vs. mass in Tr 37. The size of the filled circles and open triangles (upper limits) is proportional to the age. Very small circles represent the globule population (aged ~ 1 Myr). Ages for G-type stars tend to look larger (~ 10 Myr; G stars are marked by large open circles) but are highly uncertain. The data are consistent with the study of Calvet et al. (2004), whose data are between the dashed lines, and with the $\dot{M} \propto M^2$ trend observed by Natta et al. (2004), although our sample contains stars spanning a smaller parameter area in both accretion rate and mass. This trend appears independently of age in both the globule and the bulk (4 Myr old on average) population, even though accretion rates for the younger stars tend to be higher, as expected from the viscous disk evolution model (Hartmann et al. 1998).

円盤進化モデル計算の一例

Dullemond et al. 2006

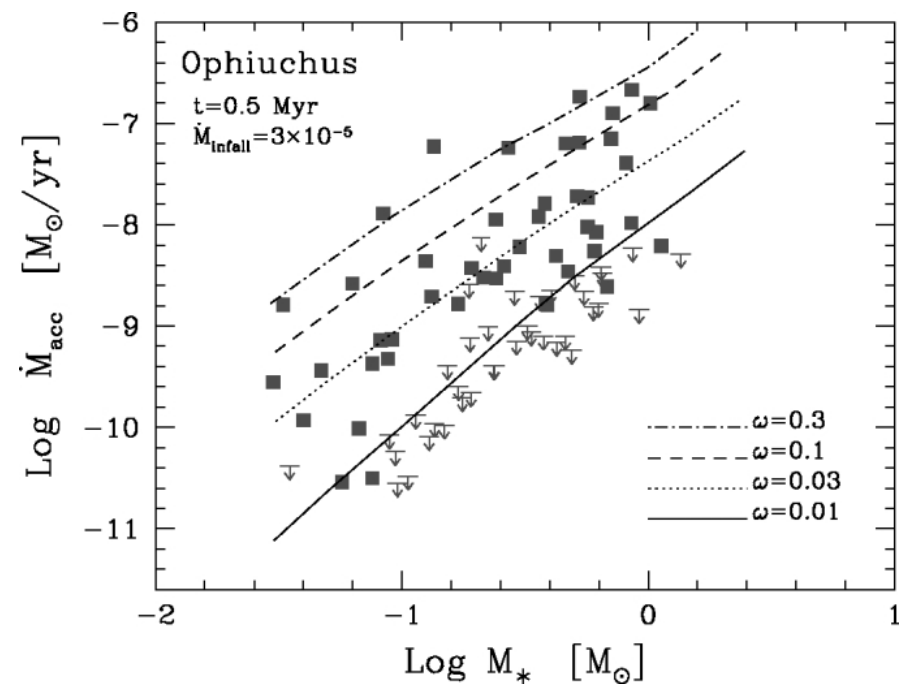
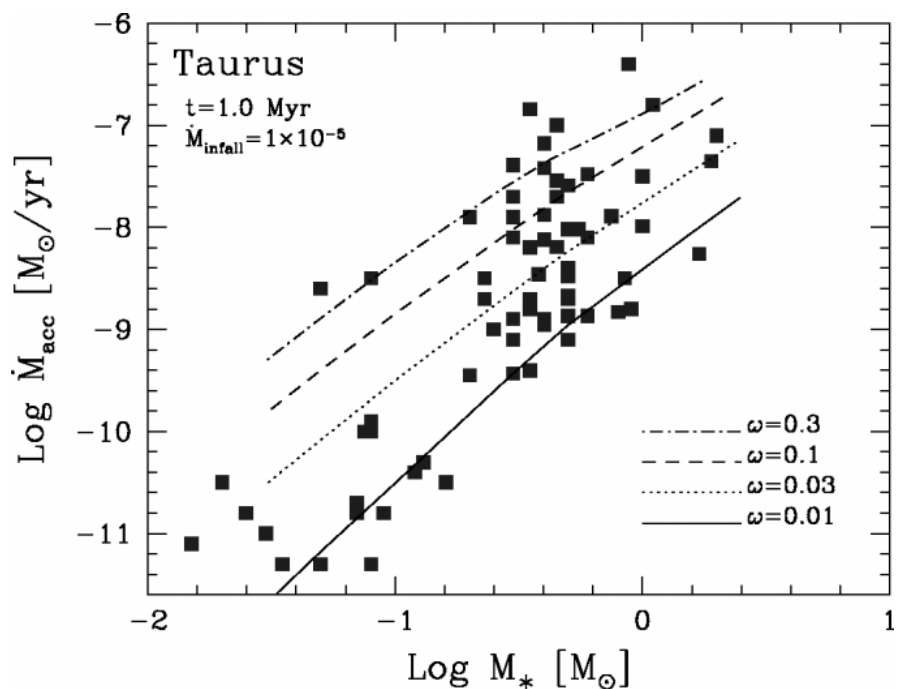


FIG. 1.—Mass accretion rate \dot{M}_{acc} as function of the mass of the central object M_* in Taurus (left panel) and ρ Oph (right panel). Symbols are measured quantities or upper limits. Each line is a model series for fixed ω , as labeled, varying M_{core} . In all model series, \dot{M}_{infall} and the snapshot time are kept constant ($10^{-5} M_{\odot} \text{ yr}^{-1}$ and 1 Myr in Taurus and $3 \times 10^{-5} M_{\odot} \text{ yr}^{-1}$ and 0.5 Myr in ρ Oph). [See the electronic edition of the Journal for a color version of this figure.]

円盤の散逸

Sicilia-Aguilar et al. 2006a

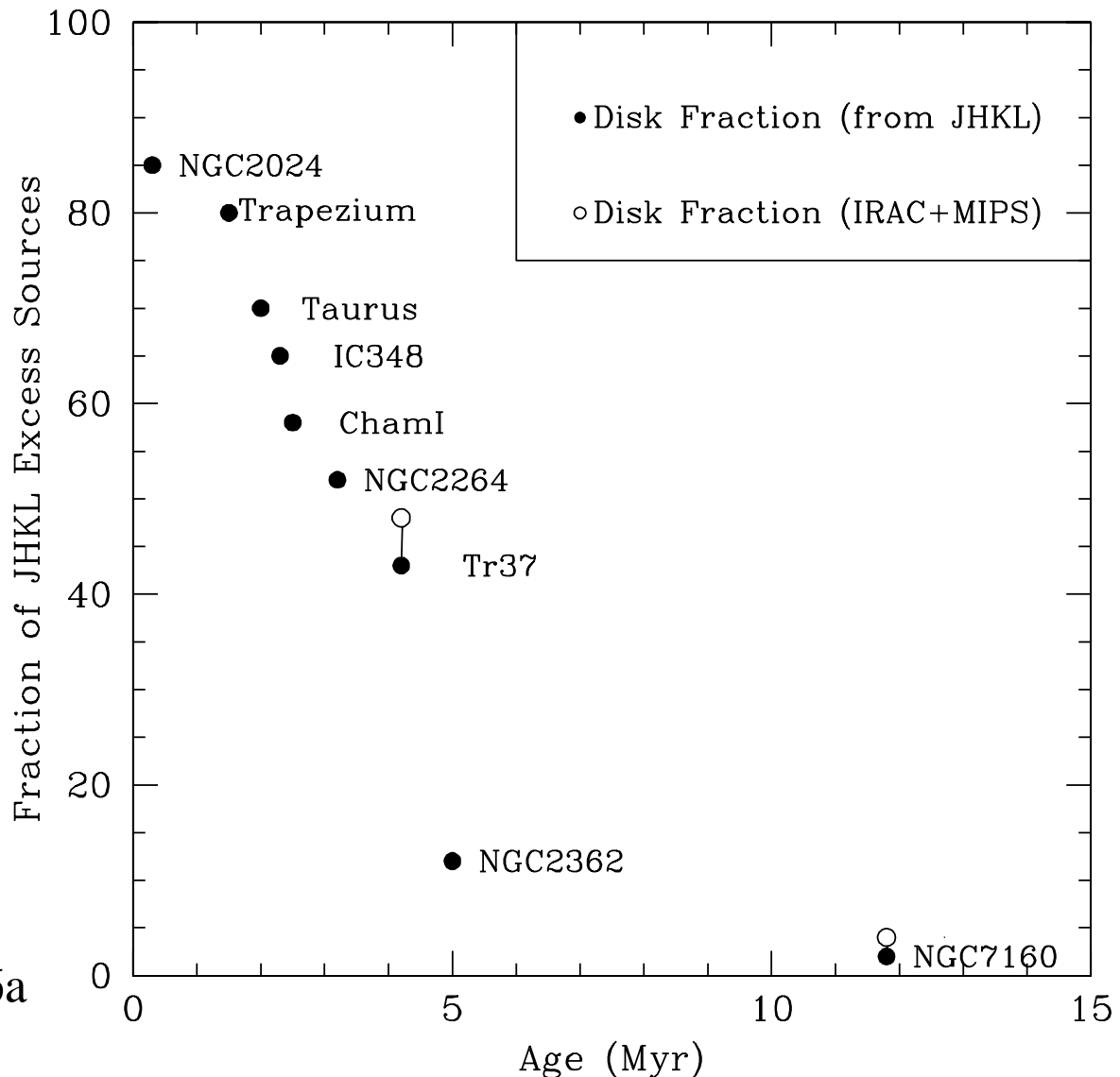


FIG. 13.—Evolution of the disk fraction (based on *JHKL* excesses) vs. age. We display the disk fraction data compiled by Haisch et al. (2001), based on the detection of *JHKL* excesses, with the disk fractions estimates in Tr 37 and NGC 48 7160, using the *JHK* and 3.6 μm excesses. We also display disk fractions esti-

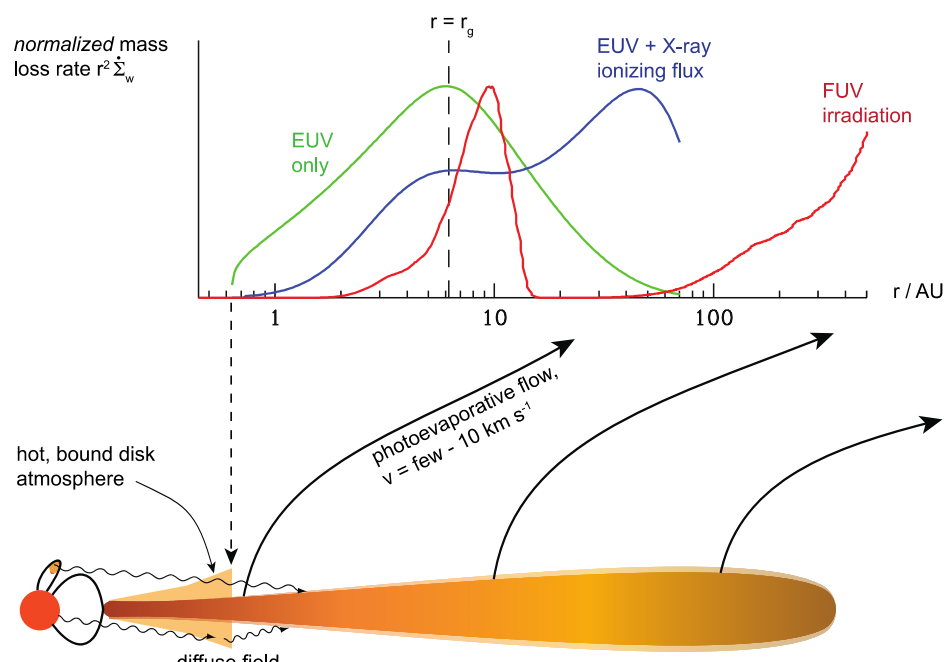
円盤ガス散逸：理論

- Photoevaporation
- Disk wind

Photoevaporation (光蒸発)

$$\frac{1}{2}v^2 - \frac{GM}{r^2} > 0$$

太陽重力圏外へ



Armitage 2011

EUV, FUV, X-ray → 電離・解離 加熱

$T \sim 10^4$ K

$$r_g = \frac{GM}{c_s^2}$$

$r > 0.1 r_g$ で有効

~ 7 AU ($1M_{\text{sun}}$ の場合)

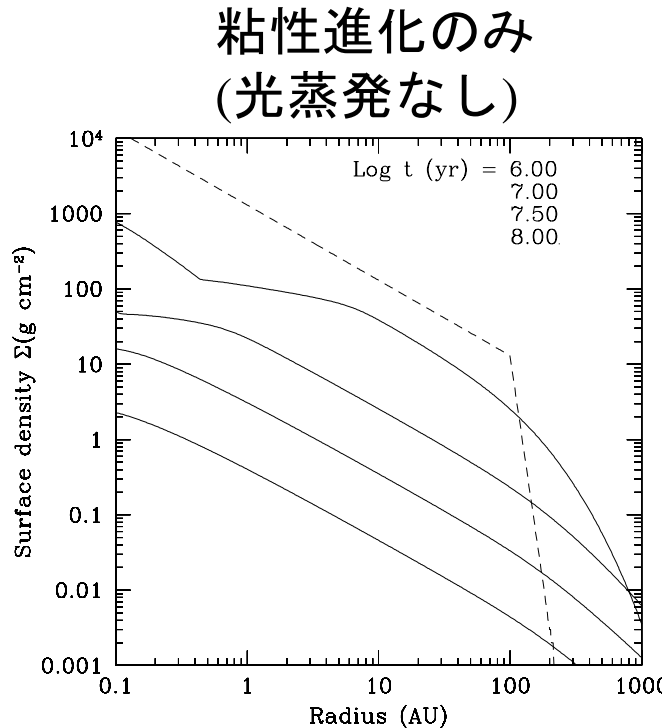


Figure 2. Surface density (Σ) distribution with time for a purely viscous disk ($\alpha = 0.01$, initial disk mass $0.1 M_{\odot}$) around a $1 M_{\odot}$ star. The dashed line shows Σ at the start of the simulation, $t = 0$. Σ with radius is shown for different instances of time indicated in the upper right-hand corner. The surface density gradually decreases with time as the disk spreads, and the disk mass is $> 10^{-3} M_{\odot}$ at 10^8 yr. The disk is optically thick to stellar photons until $\Sigma \lesssim 10^{-2}$ g cm⁻².

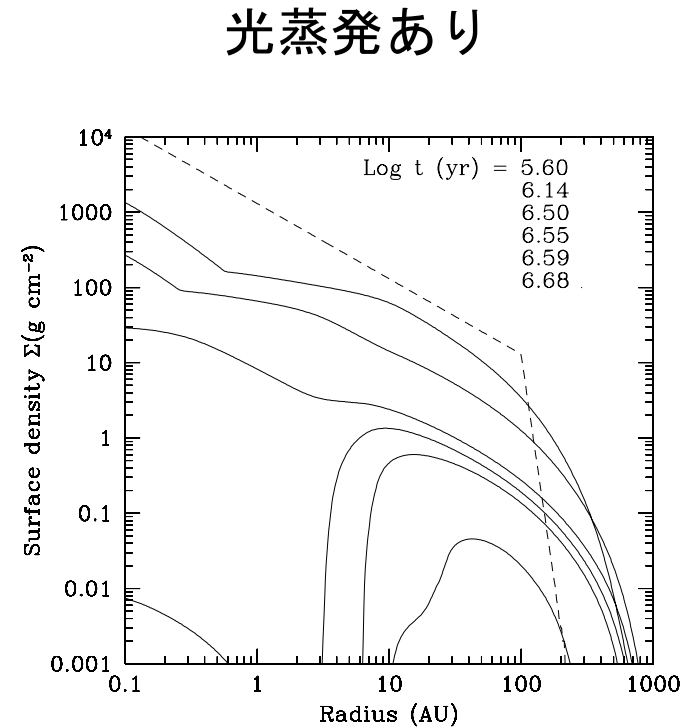


Figure 4. Evolution of the surface density distribution for the same disk/star system as Figure 2 but which is irradiated only by FUV photons ($L_{FUV} = 10^{-2}-10^{-3} L_{\odot}$, $\Phi_{EUV} = 0$, $L_X = 0$). The disk loses mass rapidly due to a combination of accretion and FUV photoevaporation and at $\sim 3.5 \times 10^6$ yr, FUV photons burn a gap in the inner disk. The disk is then photoevaporated by direct illumination of the inner gap as the outer disk continues to deplete. The remaining torus-like disk is eroded at both the inner and outer regions, while the intermediate regions survive the longest.

- Inner Hole形成
- 外側円盤も散逸
- 速い時間進化

FU Ori : 間欠的 爆発的増光

5等(=100倍)以上

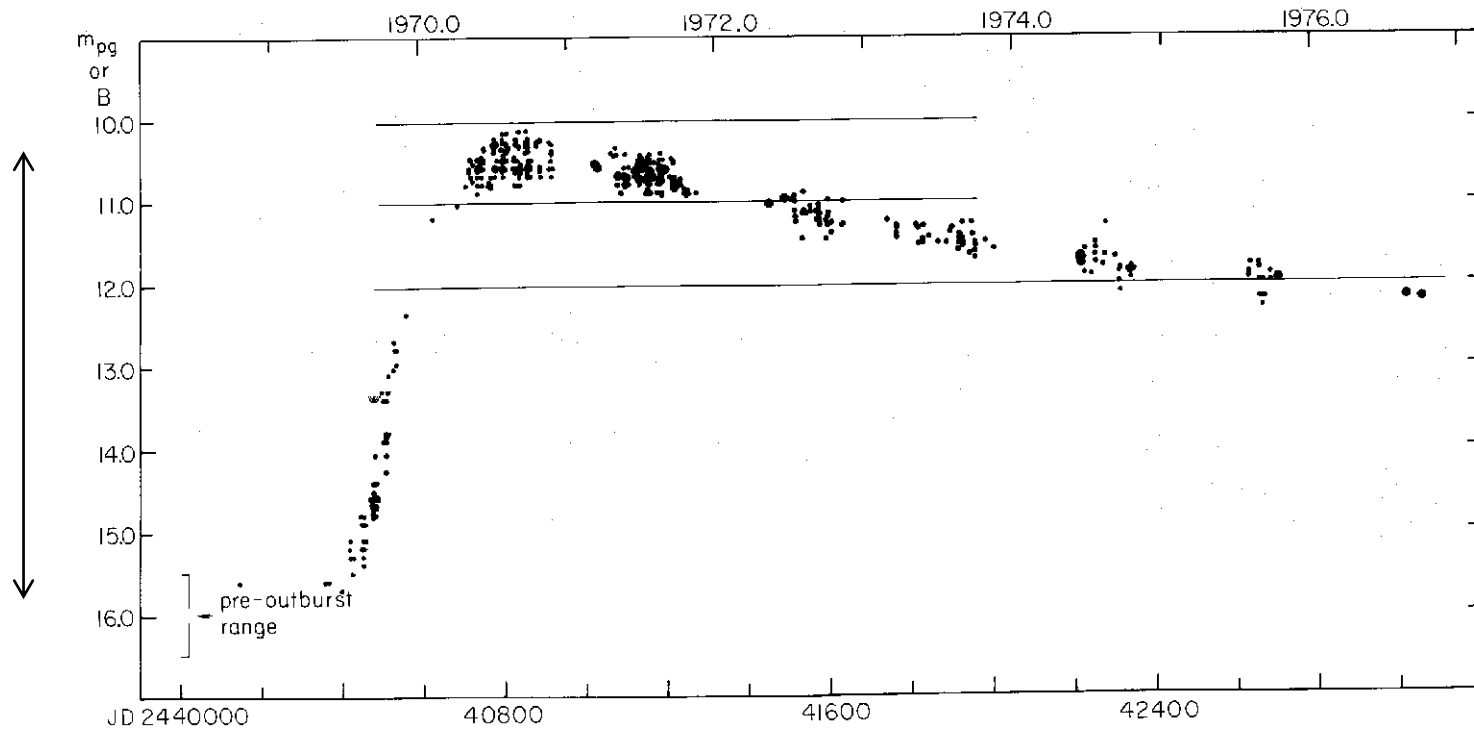
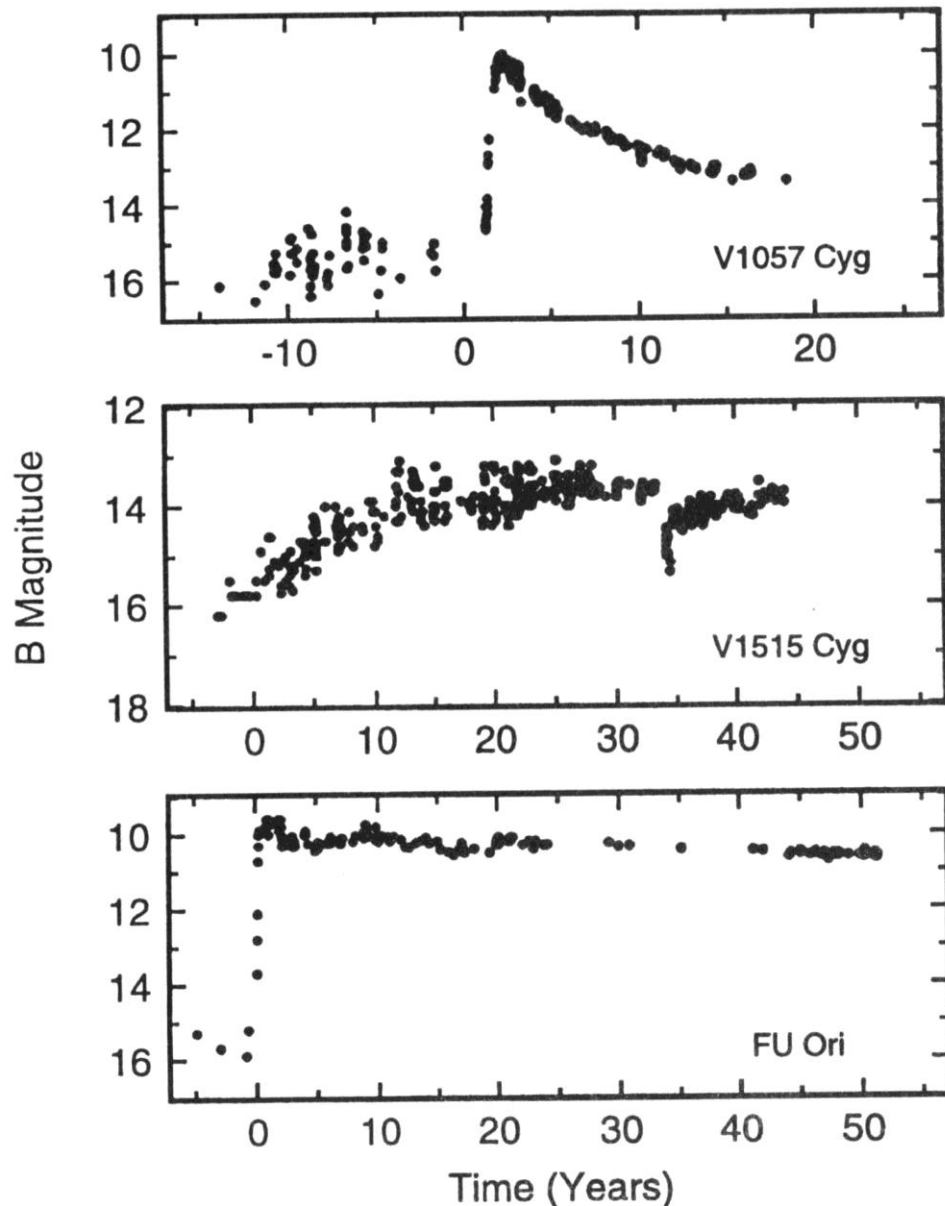


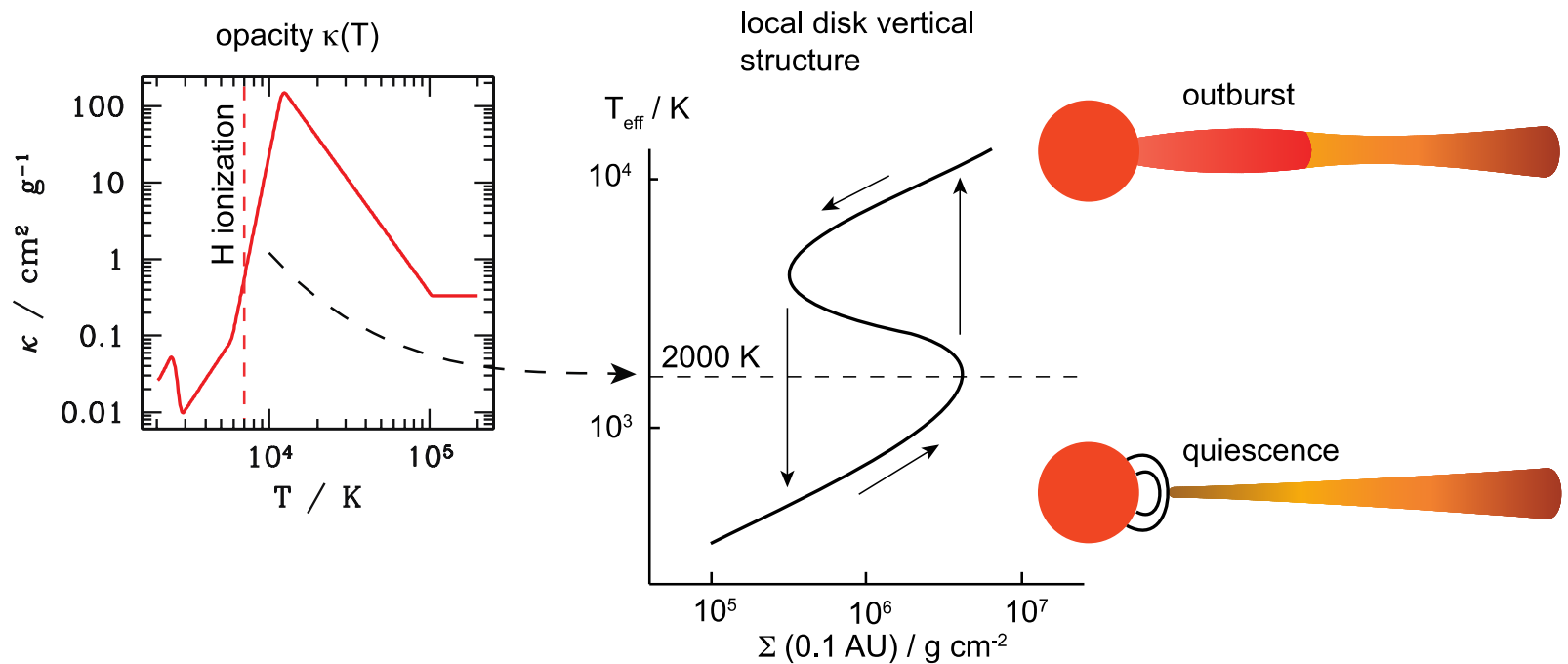
FIG. 3.—The photographic/B light curve of V1057 Cyg through 1976, compiled largely from published sources. The small points are photographic observations by Meinunger and Wenzel (1971), Giesecking (1973, 1974), Filin (1974), Landolt (1975), Mandel (1975a, b), Hoffleit (1975, private communication), and Tsvetkov (1976). The larger points are photoelectric B measurements by Mendoza (1971), Rieke *et al.* (1972), Schwartz and Snow (1972), Bossen (1972), Landolt (1975), and unpublished measures by P. Pesch, L. Cathey, and R. Stone.

Herbig 1977

FU Ori現象の観測例

Hartman & Kenyon 1996

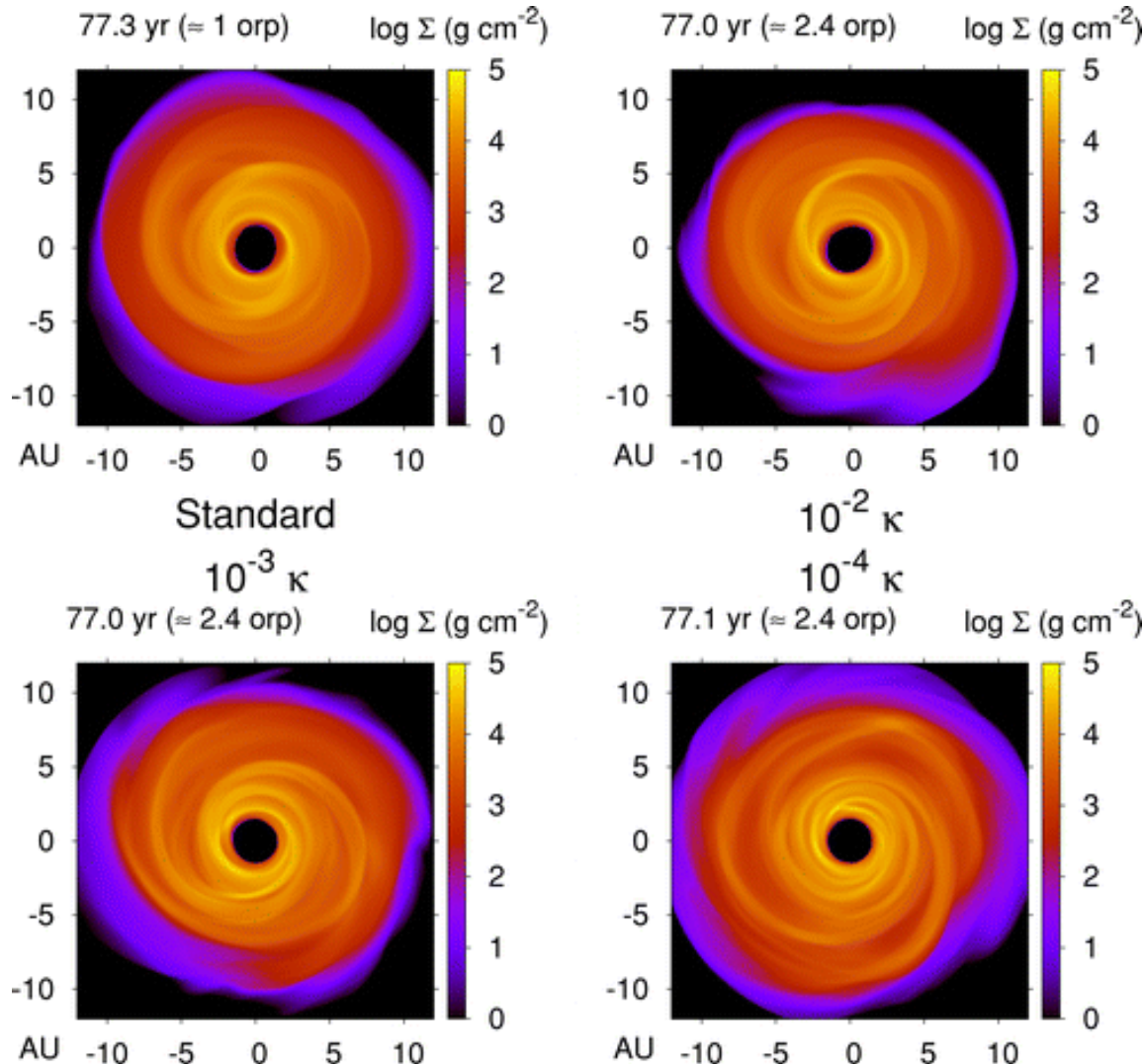




Armitage 2011

Figure 10: A classical disk thermal instability is a possibility if the accretion rate through the inner disk is such that the mid-plane temperature approaches $T \sim 10^4 \text{ K}$, at which point hydrogen becomes ionized and the opacity $\kappa(T)$ rises rapidly. Under these conditions there can be multiple solutions (an “S-curve”) for the local equilibrium vertical structure at fixed r and Σ , with the stable possibilities being a quiescent state of low accretion rate, and an outburst state with a much higher temperature and accretion rate. Provided that these states are sufficiently well-separated, it is then possible to set up a global limit cycle in which the inner disk as a whole cycles between quiescent and outburst behavior.

Dead zone → 重力不安定 → \dot{M} 增加



復元円盤

Minimum Mass Solar Nebula (MMSN) model

現在の太陽系天体が、
移動せずに形成されたとしたら？

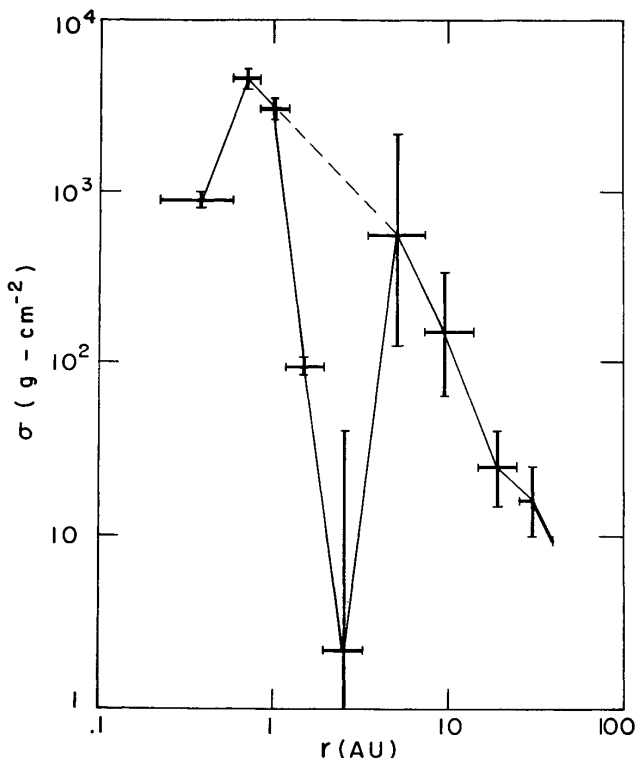


Fig. 1. Surface densities, σ , obtained by restoring the planets to solar composition and spreading the resulting masses through contiguous zones surrounding their orbits. The meaning of the ‘error bars’ is discussed in the text.

Weidenschilling 1977

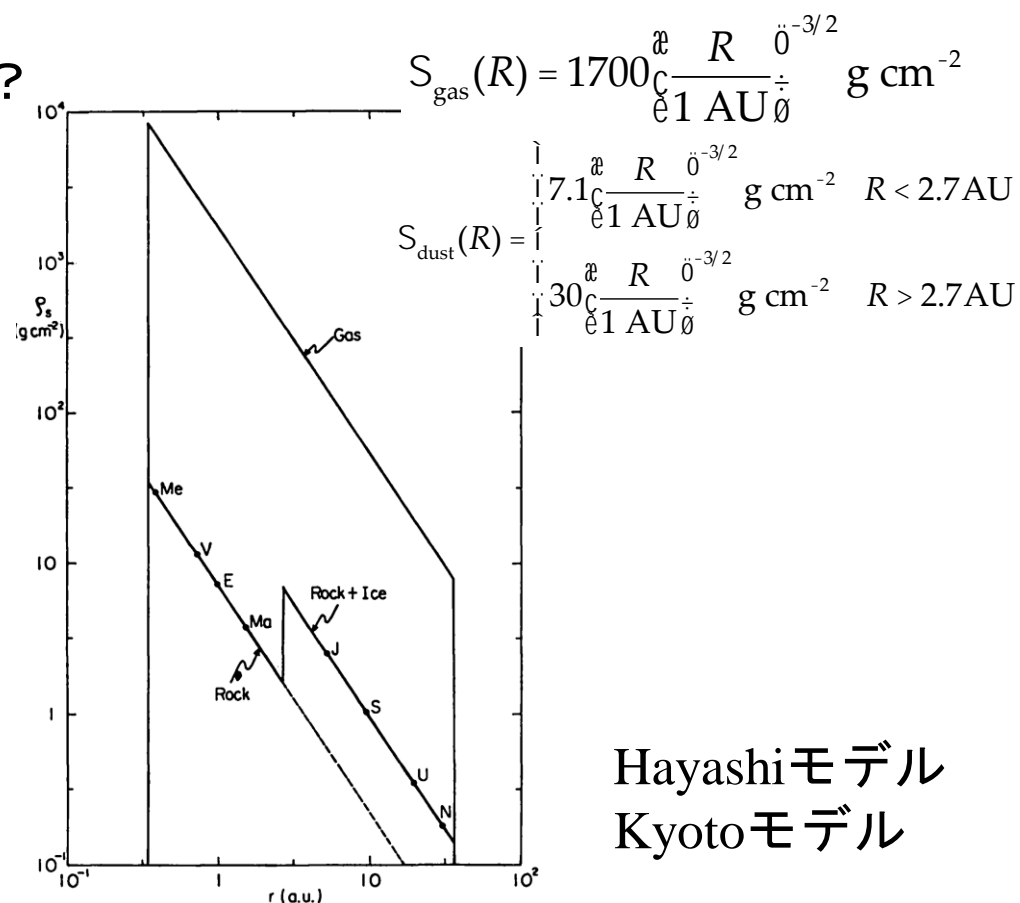


Fig. 1. Surface densities of rocky, icy and gaseous materials in the solar nebula as a function of the distance from the sun.

Hayashi 1981

Hayashi モデル
Kyoto モデル

参考文献

- Armitage, Philip J. 2011. Dynamics of Protoplanetary Disks. Annual Review of Astronomy and Astrophysics, vol. 49, issue 1, pp. 195-236
- Beckwith, Steven V. W. Sargent, Anneila I. Chini, Rolf S. Guesten, Rolf. 1990. A survey for circumstellar disks around young stellar objects. Astronomical Journal. vol. 99, March 1990, p. 924-945
- Boley, Aaron C. Durisen, Richard H. 2008. Gravitational Instabilities, Chondrule Formation, and the FU Orionis Phenomenon. The Astrophysical Journal, Volume 685, Issue 2, pp. 1193-1209
- Chiang, E. I. Goldreich, P. 1997. Spectral Energy Distributions of T Tauri Stars with Passive Circumstellar Disks. Astrophysical Journal v.490, p.368
- Chushiro Hayashi . 1981. Structure of the Solar Nebula, Growth and Decay of Magnetic Fields and Effects of Magnetic and Turbulent Viscosities on the Nebula. Progress of Theoretical Physics Supplement, No. 70, pp. 35-53
- Dullemond, C. P. Natta, A. Testi, L. 2006. Accretion in Protoplanetary Disks: The Imprint of Core Properties. The Astrophysical Journal, Volume 645, Issue 1, pp. L69-L72
- Flock, M. Dzyurkevich, N. Klahr, H. Turner, N. J. Henning, Th. 2011. Turbulence and Steady Flows in Three-dimensional Global Stratified Magnetohydrodynamic Simulations of Accretion Disks. The Astrophysical Journal, Volume 735, Issue 2, article id. 122

参考文献

- Forgan, Duncan. Rice, Ken. Cossins, Peter. Lodato, Giuseppe. 2011. The nature of angular momentum transport in radiative self-gravitating protostellar discs. Monthly Notices of the Royal Astronomical Society, Volume 410, Issue 2, pp. 994-1006.
- Gammie, Charles F. 1996. Layered Accretion in T Tauri Disks. Astrophysical Journal v.457, p.355
- George B. Rybicki. Alan P. Lightman. 1985. Radiative Processes in Astrophysics . Wiley-VCH
- Gorti, U. Dullemond, C. P. Hollenbach, D. 2009. Time Evolution of Viscous Circumstellar Disks due to Photoevaporation by Far-Ultraviolet, Extreme-Ultraviolet, and X-ray Radiation from the Central Star. The Astrophysical Journal, Volume 705, Issue 2, pp. 1237-1251
- Hartmann, Lee. Kenyon, Scott J. 1996. The FU Orionis Phenomenon. Annual Review of Astronomy and Astrophysics, Volume 34, 1996, pp. 207-240
- Hasegawa, M. Ohtsuki, K. Nakazawa, K. Nakagawa, Y. 1988. Chapter 16. Gravitational Scattering between Planetesimals and Their Statistical Behavior. Progress of Theoretical Physics Supplement, No. 96, pp. 175-195
- Hawley, John F. Balbus, Steven A. 1991. A Powerful Local Shear Instability in Weakly Magnetized Disks. II. Nonlinear Evolution. Astrophysical Journal v.376, p.223

参考文献

- Herbig, G. H. 1977. Eruptive phenomena in early stellar evolution. *Astrophysical Journal*, Part 1, vol. 217, Nov. 1, 1977, p. 693-715
- Inoue, Akio K.. Oka, Akinori. Nakamoto, Taishi. 2009. Effects of scattering and dust grain size on the temperature structure of protoplanetary discs: a three-layer approach. *Monthly Notices of the Royal Astronomical Society*, Volume 393, Issue 4, pp. 1377-1390
- Miyake, Kotaro. Nakagawa, Yoshitsugu. 1993. Effects of particle size distribution on opacity curves of protoplanetary disks around T Tauri stars. *Icarus*, vol. 106, p. 20
- Nakamoto, Taishi. Nakagawa, Yoshitsugo. 1994. Formation, early evolution, and gravitational stability of protoplanetary disks. *Astrophysical Journal*, Part 1 (ISSN 0004-637X), vol. 421, no. 2, p. 640-650
- Nishida, S. 1983. Collisional Processes of Planetesimals with a Protoplanet under the Gravity of the Proto-Sun. *Progress of Theoretical Physics*, Vol. 70, No. 1, pp. 93-105
- Oka, Akinori. Nakamoto, Taishi. Ida, Shigeru. 2011. Evolution of Snow Line in Optically Thick Protoplanetary Disks: Effects of Water Ice Opacity and Dust Grain Size. *The Astrophysical Journal*, Volume 738, Issue 2, article id. 141

参考文献

- Sano, Takayoshi. Miyama, Shoken M. Umebayashi, Toyoharu. Nakano, Takenori. 2000. Magnetorotational Instability in Protoplanetary Disks. II. Ionization State and Unstable Regions. *The Astrophysical Journal*, Volume 543, Issue 1, pp. 486-501.
- Sicilia-Aguilar, Aurora. Hartmann, Lee W. Fürész, Gábor; Henning, Thomas. Dullemond, Cornelis. Brandner, Wolfgang. 2006. High-Resolution Spectroscopy in Tr 37: Gas Accretion Evolution in Evolved Dusty Disks. *The Astronomical Journal*, Volume 132, Issue 5, pp. 2135-2155
- Sicilia-Aguilar, Aurora. Hartmann, Lee. Calvet, Nuria; Megeath, S. T. Muzerolle, James; Allen, Lori; D'Alessio, Paola. Merín, Bruno. Stauffer, John. Young, Erick. Lada, Charles. 2006. Disk Evolution in Cep OB2: Results from the Spitzer Space Telescope. *The Astrophysical Journal*, Volume 638, Issue 2, pp. 897-919
- Weidenschilling, S. J. 1977. The distribution of mass in the planetary system and solar nebula. *Astrophysics and Space Science*, vol. 51, no. 1, Sept. 1977, p. 153-158
- 柴田 一成. 松元 亮治. 福江 純. 嶺重 慎. 1999. 活動する宇宙一天体活動現象の物理. 裳華房. pp272